

NUMERICAL SIMULATION OF BPF PRESSURE PULSATION FIELD IN CENTRIFUGAL PUMPS

by

Serguei Timouchev

Director General

InteRe Ltd.

Moscow, Russia

and

Jean Turrett

Head of Acoustical Department

CETIM

Cedex, France



Serguei Timouchev is Director General with InteRe Ltd., in Moscow, Russia. He began his career in 1980 with the Buran space program, and in 1992 he began work within Moscow Aviation Institute for the Ariane-Vulcain project. Dr. Timouchev was involved in many experimental and computational studies in pressure pulsation and vibration in centrifugal turbopump units of liquid propellant rocket engines, including reduction of pressure pulsation

and vibration caused by cavitation, reverse flows, and acoustical amplification. In 1986, he proposed an original method for numerical modeling of pressure pulsation in centrifugal machines. For the last decade, he has worked on the problem of computational prediction of pressure pulsation and reduction of vibration and noise in centrifugal pumps and ventilators.

Dr. Timouchev graduated from Moscow Aviation Institute (1978) and later received his Ph.D. degree. He is author and coauthor of 30 technical papers and is an affiliate member of the INCE/Europe.



Jean Turrett is Head of the Acoustical Department, Vibration and Thermal Engineering Department of CETIM, in Cedex, France. He has been involved in the development of vectorial sound intensity, which led to the organization of four international meetings in France from 1981 to 1991. He has been active in studies on noise from hydraulic machines including pumps since 1975. Mr. Turrett developed an anechoic liquid terminator to measure

pressure pulsations in piping systems and specific methodologies to visualize acoustic wave generation inside impellers and volutes. He organized the first international meeting on fan noise in Senlis, France, in 1992, and he coorganized the First International Meeting on Pump Noise and Vibration held in Clamart, France, in 1993.

Mr. Turrett graduated from the Institut Polytechnique of Grenoble (1971). He is Vice President of the International Institute of Noise Control Engineering, President of INCE/Europe, and author and coauthor of over 40 technical papers.

ABSTRACT

There is a close link between the pressure pulsation in the pump working cavity and its vibration and noise level. Due to a current trend in increasing rotation speed and power, the problem of noise, vibration, and pressure pulsation in centrifugal pumps becomes a more urgent question. Usually the level of tone spectrum components determines the pump vibration and noise characteristics, and mainly these are blade-passing frequencies (BPF). They result from nonstationary hydrodynamic interaction between the impeller flow and pump casing. The method for computation of BPF pressure pulsations in the working cavity of a centrifugal pump is based on a representation of nonstationary motion of a compressible medium as a combination of acoustical waves and pseudosound perturbations.

INTRODUCTION—DESCRIPTION OF THE PROBLEM OF HYDRAULIC VIBRATION IN CENTRIFUGAL PUMPS

Main Noise and Vibration Sources in Centrifugal Pumps

It is well known that the principal noise and vibration sources in a well-balanced centrifugal pump are of a hydrodynamic nature. There is a close link between the pressure pulsation in the pump working cavity and its noise and vibration level.

It is possible to subdivide the nonstationary hydrodynamic phenomena in the working cavity of a pump in two groups outlined below.

- Hydrodynamic interaction between the impeller flow and the volute casing
- Vortex flow

They are accompanied by cavitation phenomena that can act as a separate source of hydraulic noise and may provoke amplification of unsteadiness of the two groups mentioned.

The first type of pressure pulsation that causes tone noise and vibration is the subject of this lecture.

Relationship Between Pressure Pulsation, Vibration, Deformation, and Noise

The conclusions drawn from the works mentioned above indicate a close link between the pressure pulsations in the pump working cavity and its vibration and noise.

The existence of intense pressure pulsations is characteristic of all types of centrifugal pumps. Under certain conditions pressure

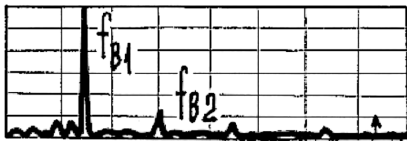
pulsations in the working cavity, e.g., in the volute casing, can achieve values dangerous to the pump integrity.

The study of pressure pulsations in the working cavity of centrifugal pumps gives information on nonstationary loads acting on the pump components—diffuser vanes, impeller blades, volute casing, outlet pipe. When measuring the dynamic load on the leading edges of diffuser vanes of a centrifugal pump by strain gauges, it was found that in the range of delivery 0.6 to 1.0 from its optimum value the dynamic load is directly proportional to the amplitude of pressure pulsations.

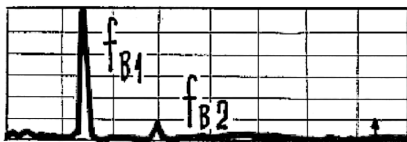
Figure 1 shows the spectra of pressure pulsations in the volute cavity, vibrations of the bladed diffuser casing, and the dynamic strain in the welded connection of the volute with the diffuser casing for a high-speed centrifugal pump. These data indicate the direct link between the pressure pulsations in the working cavity and the dynamic load acting on pump components.

It is useful to note that the level of discrete vibration spectrum components at different points of the pump casing hardly depends on its elastic-mass properties, in particular when the wavelengths of elastic deformations are comparable to the pump dimensions. Therefore, it is necessary alongside the measurement of vibration to investigate pressure pulsations in different points of the pump working cavity in order to make general and unequivocal conclusions about the influence of various factors on the hydrodynamic sources of vibration.

Deformation



Pressure pulsation



Vibration

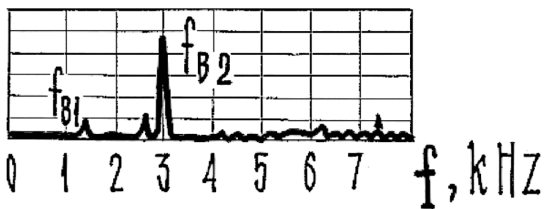


Figure 1. Frequency Spectra of a Centrifugal Pump.

Hydrodynamic Sources of Vibration and Noise

The vibration of hydrodynamic nature is related to features of the fluid flow in the pump working cavity. The nonstationary interaction of the pump casing with the flow leaving the impeller gives rise to churning (vortex-type flow generation), consisting of small-scale turbulence and large-scale rotational structures (backward flows). In addition, cavitation can develop in the working cavity of the pump.

These oscillations can be especially dangerous in the case of coincidence with the resonance frequencies of structural

components. Describing a pump with bladed diffuser as a rigid body, one can assume that vibration at blade-passing frequencies (BPF) acts as a transfer of nonstationary loads to the pump casing through the diffuser vanes. Based on the hypothesis, recommendations were made for the choice of an optimum ratio between the number of impeller and diffuser blades.

Nonstationary Phenomena and Pressure Pulsations

Characteristics of Fluid Flow and Generation of Pressure Pulsations

Pressure pulsations in the working cavity of centrifugal machines arise owing to various nonstationary hydrodynamic phenomena. The complexity of these phenomena calls for a thorough experimental and theoretical investigation of nonstationary hydrodynamics of the working cavity, taking into account such effects as the interference of pressure waves, resonance acoustic behavior of the working cavity, and others that lead to amplification of pressure pulsations.

As already stated above, it is possible to subdivide the nonstationary hydrodynamic phenomena in the working cavity of a pump, depending of their origin, into three groups:

- Hydrodynamic interaction between the impeller flow and the volute (bladed diffuser) casing
- Vortex flow
- Cavitation

The first type of nonstationary process is integrally inherent to centrifugal pumps as well as all impeller machines. It is caused by stepwise nonuniformity of flow parameters at the impeller exit. Because of nonstationary hydrodynamic interaction of this nonuniformity (rotating together with the impeller) with the casing, pressure pulsations are generated at multiple frequencies of the rotation speed.

The second type is unsteadiness caused by the vortex nature of fluid flow. The pressure in a vortex is distributed in a nonuniform fashion. Therefore, formation, separation, and displacement of vortices in the working medium cause pressure pulsations. This type of unsteadiness exists in two modes:

- Small-scale turbulence in the boundary layer and formation of turbulent sheets emanating from the structural members of the pump casing and diffuser
- Formation of large-scale vortex zones, sheet, and back flows under operation that is away from the design operation conditions

The latter concern back flows at the inducer's inlet, recirculation flows at the impeller inlet and exit, "rotational break" at the impeller inlet, secondary flows in the volute.

Cavitation appears in the nuclei of large curls and zones of recirculation flows, which in turn strengthens pressure pulsation due to the collapse of bubbles in high-pressure zones, causing erosive destruction of working blades and other structural elements.

The existence of cavitation bubbles in the zones of back flows in the pump inlet creates favorable condition for the rise of low-frequency oscillations on the order of 10 Hz, with large amplitudes throughout the pump system.

The flow recirculation at the impeller exit strengthens the pressure pulsations on the blade-passing frequency because of the amplification of flow nonuniformity and cavitation on the leading edges of diffuser vanes.

The cavitation phenomena concern the third type of nonstationary process in the pump working cavity. The cavitation arises due to insufficient head on the pump suction side, and also, as already mentioned above, in the zones of sheet flows, recirculation flows in underrated modes—at the impeller inlet and exit, and in overrated modes—in the pump volute

casing. Cavitation is an independent source of nonstationary pressure pulsations and vibration. Besides, cavitation in the impeller blade channels strengthens BPF oscillations owing to an increase of the flow pitch nonuniformity. Such a conclusion is confirmed by the outcome of visual studies of cavitating pumps.

Noise, Vibration, and Pressure Pulsation Spectra

The noise, vibration, and pressure pulsation spectra of centrifugal pumps are represented by a broadband noise to which clearly discernible discrete components are superimposed (generally, they are blade-passing frequencies). The level of these tone components mainly determines the pump noise and vibration characteristics, as the tonal noise is very uncomfortable to the human ear. These oscillations may also be harmful in the case of coincidence with the resonance frequencies of structural components or acoustical resonance of the pump working cavity. The last phenomenon is very possible for high-speed pumps of large dimension.

The small-scale vortices generate turbulent noise, which gives a broadband component of low intensity in the full frequency range of the spectra of pressure pulsation, noise, and vibration.

Large-scale vortex structures create high-level weakly correlated impulses of pressure. In the spectra of pressure pulsation, noise, and vibration, this is presented as a sharp increase of the broadband component in the zone of low and medium frequencies (called the pedestal).

Pressure Pulsations at Multiple Rotation Frequencies

Examples of typical spectra of pressure pulsations and vibration of a centrifugal pump are shown in Figures 2 and 3. They are characterized by a broadband noise component to which discrete components are superimposed. The frequencies of discrete components are multiples of the rotation frequency.



Figure 2. Spectra of Pressure Pulsations in the Volute (Above) and in the Diffuser Vane Channel (Below) of a Centrifugal Pump.

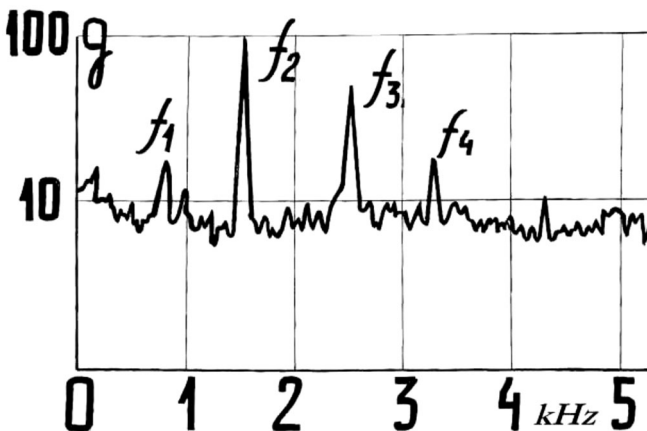


Figure 3. Typical Vibration Spectrum of a Centrifugal Pump.

• *Pressure pulsations at BPF*

Studies of centrifugal pumps show that, as a rule, the discrete BPF component and its harmonics dominate in spectra of pressure pulsations and vibrations in the design operation mode. BPF is defined by the formula:

$$f = k z f_r \tag{1}$$

where:

- f_r = Frequency of rotation, Hz
- z = Number of impeller or inducer blades
- k = Harmonic order

An investigation into the mechanisms of generation of pressure pulsations and its numerical modeling requires studies of the nature of the flow in the impeller exit zone. Increased attention in Russia and abroad has been paid during the last 40 years to experimental and computational studies of the flow in centrifugal machines. In-depth studies of the flow parameters at the impeller outlet of centrifugal pumps, compressors, and ventilators confirm that the flow in blade channels near the impeller exit can be subdivided in two areas—a high-energy jet component and a low-energy zone of vortex sheets. Such flow characteristics induce an essential pitch nonuniformity of relative and absolute velocities and flow angles, as the low-energy zone adheres to the suction side of the blade. On the impeller exit, the pitch distribution of the static pressure is close to uniform; therefore, the difference in total fluid energy between the two mainly originates from the dynamic part of the fluid energy. Due to the heterogeneity of flow in the presence of the passing impeller blades, a pressure variation in each channel of the diffuser or in the volute takes place.

Especially sharp flow variation occurs near the leading edges of diffuser vanes and volute tongue. Consequently, great attention must be given to the choice of an optimum radial gap between the impeller and diffuser vanes or volute tongue.

As specified previously, the separation of nonstationary pump processes is conditional on three types. Therefore, the formation of curls and cavitation in blade channels of the impeller strengthens the pitch nonuniformity of flow and promotes amplification of BPF pulsation. The recirculation of flow on the impeller outlet also strengthens the unsteadiness of the first type; because it is known that the same design measures reduce BPF pressure pulsation and recirculation of flow at the impeller outlet. Flow separations and cavitation in pump casing can be in turn periodically initiated by the passage of impeller blades.

Thus, the unsteadiness of the first type (hydrodynamic interaction between the impeller flow and the casing) takes a special place in the vibration character of a centrifugal pump. Determination of its vibration and noise in the optimum operation mode is the most important object of study for reduction of BPF pressure pulsations and vibration and increase of lifetime with preservation of high power characteristics.

• *Pressure pulsations at the rotation frequency*

Manufacturing deviations of impeller geometry with respect to the angular symmetry and the asymmetrical disposition of the impeller and inducer blades give rise to pressure pulsations at the rotation frequency and its higher harmonics. This is explained by tangential nonuniformity in the distribution of flow parameters at the impeller exit circle. Rotating together with the impeller, this nonuniformity excites oscillations with the rotation frequency in the pump volute or diffuser vane channels.

• *Combined components in the pressure pulsation spectra of a centrifugal pump with inducer*

An essential role in the formation of the flow pitch nonuniformity at the impeller outlet belongs to Coriolis and centrifugal forces. It results in a nonlinear character of interaction of the initial nonuniformity of the flow, caused by the inducer, with an irregular flow in the impeller. In other words, pitch nonuniformity of the flow

in the impeller channels is modulated by the “inducer” pitch nonuniformity. The frequencies of this modulation are:

$$f_m = f_r (m z_i \pm z_a), \quad m = 1, 2, 3, \dots \quad (2)$$

where z_a is the number of inducer blades.

For example, in a centrifugal pump with a double-bladed centrifugal impeller having seven main and seven additional short blades and three-blade inducer in the spectra of pressure pulsations (refer to Figure 2), the combined frequencies account for 4, 10, 11, 17, 18, and 24 multiples of the rotation speed.

Considering this, it is possible to shape the spectra of pressure pulsations and vibration of the centrifugal pump by design. The application of a centrifugal impeller with six main blades instead of seven in the same pump eliminates such discrete components as $4f_r$.

• *Possibilities of diagnosing pump operability by measuring pressure pulsations*

The pressure pulsations in the pump working cavity can be a useful indication for the diagnosis of the availability of the unit as well as of dangerous operational modes—cavitation in particular. While the signal coming from the vibration transducer is influenced by mechanical properties of the installation setup, the pressure pulsation sensor immediately reflects any change of physical parameters of the working medium.

Experimental and computational studies have shown the possibilities of diagnosing centrifugal pump impeller breakage and approaching critical cavitation operation mode of axial pumps.

Dependence of Pressure Pulsations, Vibration, and Noise on Operational Mode and Design Features

Influence of Flow Rate

As a rule, the peak-to-peak level of the total signal of pressure pulsations is at minimum near the optimum delivery and that it considerably increased at flow rates that deviate from this optimum. The minimum of pressure pulsations does not necessarily precisely coincide with the optimum point of the power performance of the pump. In the range of flow rates of about 0.8 to 1.1 of the BEP value, the level of pulsations is low. By decreasing the flow rate, the pressure pulsation level rises due to the amplification of pitch nonuniformity of the outlet impeller flow due to the contraction of the zone of active flow and the amplification of vorticity. A number of works have shown that, at lower flow rates, the low-frequency component of pulsation spectrum increases.

In conditions of insufficient suction head at low flow rates, the probability of initiation of low-frequency auto-oscillations of the hydraulic circuit is increased.

At higher flow rates, the pressure pulsations increase due to separation of flow and development of cavitation on diffuser vanes near the volute throat. With the flow rate increasing, the total level of pressure pulsation can also rise at the expense of BPF pulsations.

Pressure Pulsations in Various Elements of the Hydraulic Circuit

The indicated features of the change of pressure pulsation due to the flow rate variation are characteristic of different points of the hydraulic circuit of centrifugal pumps. The pressure pulsations were investigated at the input of a pump, in the channels of a centrifugal impeller, at the impeller outlet, in the vaneless diffusers, in the bladed diffuser channels, in the volute and conic diffuser, in seals and bearings, and in the outlet pipe.

These studies show that at operation mode close to optimum, BPF discrete components dominate the pressure pulsation spectra. The maximum amplitude of pressure pulsations was observed immediately at the impeller exit. For a rough estimation one can

assume that around the best efficiency point the amplitude of pressure pulsation in the outlet pipe makes less than 5 percent of the pump head, and in a working cavity of the pump the amplitude can reach more than 10 percent of the pump head.

Influence of Rotation Speed

Experience shows that in the absence of cavitation and resonance the amplitude of pressure pulsations, vibration, and noise of a centrifugal pump rises proportionally to the two to three power of the rotation speed.

It is known that the nonstationary flow generates acoustic waves. The periodic changes of flow parameters in the pump casing not only causes nonstationary loads on structural elements of the circuit, but will also generate acoustic oscillations, which propagate in the working medium with the speed of sound. In modern high-speed pumps, the length of acoustic waves can be comparable to the size of the circuit elements. Therefore, the variation of rotation speed can substantially modify the amplitudes of pressure pulsations in dependence of matching between characteristic driving frequencies (multiples of the rotation frequency) and the resonance frequencies of the circuit.

The amplification of pressure pulsations can happen due to matching of frequencies of oscillations with acoustic resonance frequencies of both the pipeline and the volute, i.e., the working cavity.

The behavior of BPF amplitude in the outlet pipe considerably depends on the exit impedance boundary condition. On the other side, experiment shows that pressure pulsation in the pump cavity is not affected much by the impedance of the outlet pipe.

Influence of Positive Suction Head (at the Pump Inlet)

By decreasing the positive suction head down to first critical mode, pressure pulsations at the inlet and the outlet of the pump do not change much. Study of pressure pulsations in various points of a centrifugal pump operating in cavitation mode, and comparison with published data of cavitation tests of pumps including visual research, shows that with inlet pressure decrease and formation of cavitation zones on the edges of working blades, the flow pitch nonuniformity at the impeller exit amplifies. It results in a magnification of BPF amplitude of pressure pulsations in the pump volute casing and outlet pipe. For a two-row impeller this applies to the main long blades, while the parameters of the flow in the short blade channels vary insignificantly, and the BPF amplitude of pressure pulsations relative to the total number of blades does not vary down to second critical mode.

Figure 4 and Figure 5 show the amplitudes of pressure pulsations against the pump inlet pressure at the optimum operational mode. The cavitation performance of the pump is shown in Figure 4. From these data, it is visible that in cavitation conditions the pressure oscillation level increases in the pressure tract of the pump. On the contrary, at the pump inlet the pressure pulsations drop as an effect of a weak acoustic conductivity of the vapor-gas bubbles. Figure 5 shows BPF amplitude at different rates ranging from 0.65 up to 1.15 of the optimum value. In the zone of the second critical mode, the levels of total signal and BPF pressure pulsations sharply increase and drop only for a deep collapse of the pump.

Influence of Design Features of a Centrifugal Pump

The most effective way of lowering hydrodynamic vibrations of a pump is to apply a number of measures directed to reduction of pressure pulsations at the source of oscillations, which is directly in the working cavity of the pump.

Experience shows that the amplitudes of BPF pressure pulsations depend on several design factors—form, number and disposition of blades of the impeller and the diffuser, configuration of the volute, and radial gap between the impeller and the bladed diffuser or the volute tongue (cutwater).

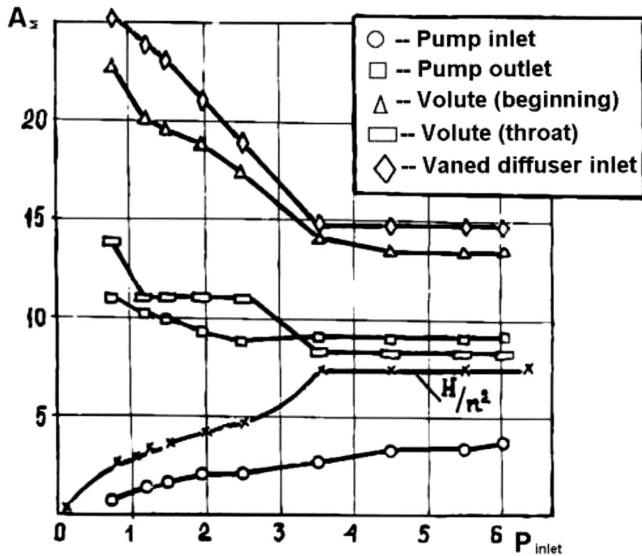


Figure 4. Pressure Pulsations in a High-Speed Centrifugal Pump with Inducer: Dependence of the Total Signal Amplitude on the Pump Inlet Pressure.

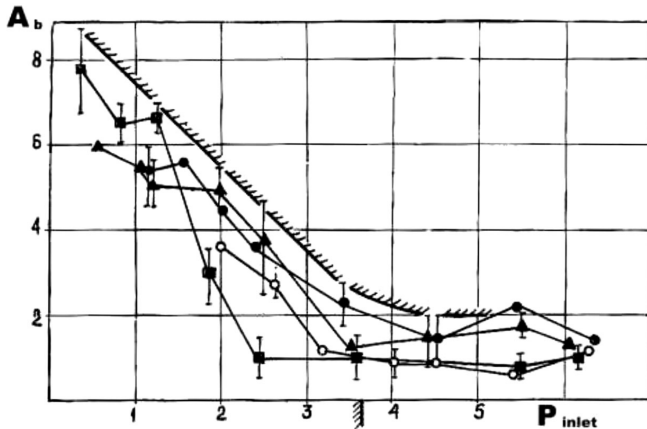


Figure 5. Pressure Pulsations in a High-Speed Centrifugal Pump with Inducer: Dependence of the Base BPF Component Amplitude at the Impeller Exit on the Pump Inlet Pressure.

- Influence of radial gap

Radial gap between impeller and volute tongue or bladed diffuser inlet is an important parameter influencing pressure pulsation in a centrifugal hydraulic machine. It is defined as:

$$\delta = (D_3 - D_2) / D_2 \quad (3)$$

Usually it is expressed in percentage of impeller tip diameter D_2 or radius R_2 . Consequently, D_3 or R_3 relates to the lower edge of the tongue or inlet of the vaned diffuser. The radial gap is one of the parameters influencing the intensity of hydrodynamic interaction between the impeller and the pump casing. Therefore, the magnification of the radial gap ensures, as a rule, reduction of all BPF discrete components in the spectra of pressure pulsations and vibration. The practically total absence of discrete components in the pressure pulsation spectrum of a centrifugal pump with vaneless diffuser was observed under $D_4/D_2 = 1.4$, where D_4 was the outside diffuser diameter. This corresponds to a gap between the impeller and tongue equal to 0.45 of the blade pitch on the impeller external diameter. Just such a distance is required for the disintegration of a large-scale vortex, which flows out from the working cascade. It is no wonder, therefore, that

research indicates an exponential growth of pressure pulsations with radial approach to the tip impeller radius. In practice, the necessary gap is ensured by cutting of the impeller and (or) diffuser vanes/volute tongue, which is most effective for small initial gaps (1.0 to 1.5 percent). An increase of the radial gap more than 5 percent is not so effective and can also make the pump head performance worse. The pressure pulsations can even increase in case of aggravation of the flow conditions in the diffuser vane cascade. Therefore, it is preferable to select an optimum radial gap at the design stage.

- Influence of geometry of the impeller

Experimental studies show the tendency of reduction of pressure pulsations with a reasonable increase in number of blades of the impeller. However, it is necessary to avoid resonance of pressure pulsations due to matching of BPF with resonance frequencies of pipelines or pump working cavity. To reduce overload in the impeller inlet region, two and three row centrifugal impellers are made with additional short blades. Significant reduction of pitch nonuniformity of flow can be achieved by the separation of the centrifugal impeller by partitions in the meridional plane and angular shift of blade channels.

It is well known that increase of the exit blade angle of a centrifugal impeller leads to magnification of pressure pulsations. The greatest pressure pulsations are created by centrifugal impellers with forward bent radial blades. In the range of small angles (10 to 30 degrees), pressure pulsations practically do not depend on the blade exit angle. The only way to improve prediction capabilities is the inclusion of impeller flow computation into the procedure of numerical modeling of pressure pulsations.

- Influence of pump casing design

From experimental data it is known that the lowest level of vibration occurs in pumps with a vaneless diffuser having $D_4/D_2 = 1.35$ to 1.45, where the radial size of the pump is increased at the expense of reduced efficiency. Application of a so-called "sided volute" is therefore recommended, accompanied by an efficiency decrease of 1 to 1.5 percent. A bevel of volute tongue with an angle of 30 to 45 degrees is widely practiced, as it allows smoothing out of the blade-passing impulse. These measures, as well as influence of the geometry of the bladed diffuser and use of damping devices in the volute, require an appropriate computational prediction.

Review of publications indicates that experimental studies have accumulated considerable material on the problem of pump vibration and noise. However, it is not possible to make strict recommendations for designers and manufacturers by generalizing these data in a straightforward manner because of their incompleteness or peculiarity. At the same time, this problem is of a complex character. It requires numerical computation based on a theoretical model of pressure pulsation generation by a direct solution of the main equations of motion of the working medium in a given pump configuration.

Review of State-of-the-Art of Pressure Pulsation Computation

Nowadays the need has increased to have the ability to determine by computation the level of pressure pulsations in a hydraulic circuit during the design stage and to outline design alternatives. However, until recently, reliable methods were not developed despite significant progress in the methods of computational hydrodynamics. This is related to difficulties in the construction of an adequate mathematical model of the phenomenon that could allow the creation of an effective computer code.

The computational determination of pressure pulsations allows selecting the design variant at the design stage that ensures the lowest vibration while still maintaining the specific power parameters, and also evaluates nonstationary loads acting on the structural elements of the circuit.

Computational Model of Joffe-Panchenko

This model is the first attempt to treat the problem of hydraulic vibration in centrifugal pumps with a vaned diffuser. One important problem of pump design is the choice of the optimum number of impeller blades z_1 and of a vaned diffuser z_2 . For a certain unfavorable ratio z_1/z_2 , the amplification of BPF oscillations or its harmonics can occur. In the Joffe-Panchenko (1972) model, dynamic forces acting on diffuser vanes cause BPF vibration. Such forces can be represented as a Fourier series.

Factors of such a series depend on the assumed function of force variation with time (density of the working fluid, profile of flow velocities, geometric parameters of the blade cascade, gap between the impeller and diffuser, etc.).

The optimum ratio of numbers of blades is selected so that the dynamic force and moment obtained by summation over all diffuser vanes are at a minimum. The fulfillment of the two inequalities for the first three to four harmonics requires that:

$$\frac{kz_1 \pm 1}{z_2} \neq J; \quad \frac{kz_1}{z_2} \neq J \quad (4)$$

where:

k = Harmonic order

J = Positive integer

This model is correct when a pump case vibrates as a rigid body. Besides, an important factor like pressure pulsations in the pump working cavity is not taken into account here.

The main conclusion derived from this theory is that the source of pulsations in a centrifugal pump has a determined spatial structure.

Computational Model of Chen

For the first time a computational model for the determination of BPF pressure pulsations in the volute casing of a centrifugal pump with a vane diffuser was created by Chen (1961). The computational model of Chen imitates the volute casing with a vaned diffuser: vaned channels of the diffuser and of the volute are substituted by tubes of constant cross section. The boundary conditions at the vane channel inlet of the diffuser are given as acoustic perturbations of pressure and velocity.

At the diffuser channel exit the condition of flow continuity is imposed. At the beginning of volute and in the throttle, cut T and O in Figure 6, the boundary conditions are determined by the appropriate reflection coefficients.

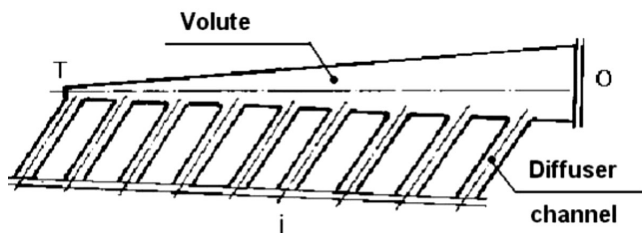


Figure 6. Computational Model of Chen.

In this work, the linearized one-dimensional wave equation of oscillations in the volute is presented. The solution is noted in terms of direct and reflected waves propagating toward the throttle section and in the opposite direction, respectively. The formulae for the determination of amplitudes of pressure pulsations have been obtained. However, for the realization of calculations using these formulae, it is necessary to know the magnitude of velocity oscillations at the exit of the vane channel of the diffuser. Determination of velocity pulsations is a complicated hydrodynamic problem, which in the quoted work has not been solved. Consequently, no quantitative result was obtained.

On a qualitative level such an approach allows identification of an approximate criterion of resonance of pressure pulsations in the volute as the interference of acoustic waves originating in different channels of a diffuser is implied in the model. However, a similar result can be obtained in a simpler way only from the analysis of phase relations for pressure impulses.

So-called "backward wave resonance" in the initial cross section of the volute occurs when:

$$\frac{z_2 - z_1}{z_2} \left(1 - \frac{\pi f_r D_m}{a - U_m} \frac{z_1}{z_2 - z_1} \right) = + \frac{J}{k} \quad (5)$$

"Direct wave resonance" will take place according to Chen (1961) when:

$$\frac{z_2 - z_1}{z_2} \left(1 + \frac{\pi f_r D_m}{a - U_m} \frac{z_1}{z_2 - z_1} \right) = - \frac{J}{k} \quad (6)$$

where:

f_r = Frequency of rotation, Hz

D_m = Average diameter of the volute

U_m = Average flow velocity of the fluid within the volute

a = Average speed of sound

k = Harmonic number

J = ... -3, -2, -1, 0, +1, +2, +3

Any further development of this method would not provide the possibility of accounting for influence of pump geometry on absolute values of pressure pulsations. This theory gives an example of pure acoustical method of solution of the problem of determination of pressure pulsation.

Computational Model of Sukup and Other Semiempirical Models

As already mentioned above, for the determination of amplitudes of pressure BPF oscillations in a pump casing, it is necessary to know the distribution of flow parameters in the relative motion on the pitch of the impeller exit radius.

With the approximation of potential two-dimensional flow of an ideal fluid, such a problem was addressed by Sukup (1974, 1975). It was proposed that at the exit of each impeller channel, the flow consisted of an active zone and a zone of return flow. Thus due to passing of working blades relative to diffuser channels, at the inlet of the latter there are pulsations of delivery, which can result in velocity and pressure fluctuations.

This method has two serious defects. First, the application of the potential flow theory gives in essence an incorrect picture of relative velocity distribution across the pitch of the working cascade. Second, a rough simplification of the mathematical model of generation of pressure pulsations is made: the amplitude of pressure pulsation is directly proportional to the amplitude of velocity pulsations in the absolute motion at the diffuser input. Nevertheless, this theory brings the idea of unsteady boundary condition as a rotating velocity profile at the impeller exit.

Various semiempirical laws can certainly render a great favor in an engineer's work. Such laws may link relative amplitude of pressure pulsations at the output (exit) of the centrifugal pump to the operation mode and design factors. However, they can have only limited application for similar pumps. Besides, they do not give any information about the level of pressure pulsations immediately in the pump working cavity and do not take into account the possibility of emergence of acoustic resonance in the hydraulic circuit.

"Direct Solution" Method

Some works were published in which the methods of prediction of pressure pulsations were developed by a direct computation of nonstationary two-dimensional flow in a centrifugal impeller and volute with solution of averaged Navier-Stokes equations and k-ε

models of turbulence. Other approaches used solutions of hydrodynamic equations accompanied by laser anemometric measurements.

Computation of pressure pulsation by resolving the equations of hydrodynamics as developed by Croba and Kueny (1992) and Croba, et al. (1993), offer a method of computation of nonstationary two-dimensional flow in a centrifugal impeller and volute with solution of average Navier-Stokes equations and $k-\epsilon$ models of turbulence. The computation is carried out by a direct method on two different grids—for the impeller and the volute. The transfer of parameters from one area into the other is carried out with the help of a bilinear interpolation in the zone of overlapping of finite difference grids (so-called “sliding grids”). In this method, the essential difficulty in defining the pressure-boundary-condition at the volute (pump) outlet is not overcome. Namely, this is assumed to be constant, though it is obvious that the downstream pressure oscillates at the blade-passing frequency. There is no possibility of computing correct amplitude of pressure pulsations in the outlet part of the volute and in the conical diffuser of the centrifugal pump. Simply it is the result of application of the model of incompressible liquid.

Another approach using the Reynolds equations is offered in the work by Chu, et al. (1993). The nonstationary pressure in a volute is determined by integrating Equation (7).

$$\frac{\partial p}{\partial x_i} = -\rho \left[\frac{\partial u_i}{\partial t} + u_j \frac{\partial u_i}{\partial x_j} + \frac{\partial}{\partial x_j} (\overline{u'_i u'_j}) \right] \quad (7)$$

Here all the members in the right part are determined experimentally by a laser anemometric method.

A similar approach has been developed in a work of Thompson, et al. (1992), where the laser anemometric method was also used, but the pressure pulsations are calculated by the resolution of Equation (8):

$$\left(\frac{\partial^2}{c^2 \partial t^2} - \nabla^2 \right) i^* = \text{div}(\nabla \times v \times v) \quad (8)$$

where:

$$i^* = \int \frac{dp}{\rho} + \frac{1}{2} v^2 = \text{Full enthalpy of the fluid}$$

v = Fluid velocity

Certainly unsteady phenomena in centrifugal pumps can be treated by modern computational fluid dynamics (CFD) by using some direct unsteady computational procedure. But it will not be the easiest approach. In the flow part of the pump casing, there are two modes even two zones of perturbations, which differ in the physical nature of oscillations and equations describing their behavior. The first mode is pseudosound oscillation caused by the unsteady vortex motion of liquid as an incompressible fluid. These oscillations occur only near the impeller. The velocity of propagation of the disturbances is equal to the main flow velocity; they are described by the nonlinear equations of parabolic-elliptical type. The second mode is the acoustic oscillation, which extends throughout the entire zone of flow with the speed of sound; they are governed by a linear hyperbolic equation.

Taking into account the latter fact, CFD simulation of oscillations in the centrifugal pump (even in any pump) must be based on an explicit numerical algorithm. The need for stability of such an algorithm requires a severe limitation to the time step of computation. In this case, the time step of computation is proportional to the square of step of space grid and to the square of Helmholtz number. It gives at least three orders less value of time step than Courant's condition requires. On the other side, the finite-difference grid in the zone of pseudosound oscillation must be sufficiently fine in order to ensure the correct phase resolution of unsteady flow in the presence of high gradients of outlet velocity at the exit of blade cascade of the impeller.

This entire set of conditions leads to the fact that modern three-dimensional (3D) network simulator (NS) CFD codes for compressible fluid prove to be ineffective for solving the problem of optimizing the design regarding pressure pulsation and noise.

Regarding existing 3D NS codes, there will be the following main difficulties:

- Acoustic fluctuations of pressure are significantly less than pressure differentials in the environment due to the mean flow; therefore, the acoustic part of the pressure will have large errors because of the roundoff errors of a computer.
- Direct approach will require the solution of the equations of transfer for the wave, and the numerical schemes of second and third order have large scheme diffusion and dispersion, which will cause the strong nonphysical damping of the solution and the appearance of new parasitic acoustic harmonics. After 50 to 100 iterations the wave package, which initially has the form of step on 10 mesh cells, spreads to 20 cells and has a form of hump (semisinus), which indicates a complete filtration of high-frequency harmonics.
- During the direct solution it is necessary to solve four equations—three for velocity and one for pressure—with the use of a comprehensive grid (minimum of six cells for the length of shortest disturbance), which will lead to high expenditures of processing time.

For the solution of this problem a method is proposed that is based on splitting the equations of compressible fluid dynamics into two modes—vortex and acoustic. In this case nonlinear equations for unsteady vortex motion of an incompressible liquid are solved with a bigger time step. Wave equation relative to the pressure pulsation that takes into account acoustic impedance on the boundaries of computational domain is solved by a highly effective explicit method. As a result, the whole processor time for both modes of oscillations is reduced.

Developed in six years by the authors' companies, a specialized software package became a useful tool for designers and researchers in the field of vibration and noise problems in centrifugal pumps and ventilators.

THEORETICAL BACKGROUND OF THE ACOUSTIC-VORTEX METHOD

Physical Nature of Generation of BPF Oscillations

BPF pressure pulsation and tone noise and vibration are generated by a stepwise nonuniformity of flow parameters at the centrifugal impeller exit that causes vortex perturbations. These perturbations result from the motion of periodically inhomogeneous flow with a peripheral velocity U_2 of the impeller relatively to the pump casing. Convective transposition of vortex perturbations is considered as the main physical reason of nonstationary generation process of BPF pressure pulsations in the pump. It is well known that the pressure pulsation field in the working cavity of a centrifugal pump or ventilator may be represented as a combination of pseudosound oscillations (“vortex mode”) and acoustic waves (“acoustic mode”). The vortex perturbations exponentially damp in the limits of the zone, whose dimension in order of magnitude is equal to the characteristic vortex size. They generate acoustic oscillations propagating in the pump working cavity and the outlet pipe with the speed of sound.

For better understanding of pulsation generation, let us consider a simplified model—a half-infinite pipe. At the pipe inlet there is a velocity profile C that moves with the speed U relatively to the pipe. Consider three main cases:

1. $U \ll C$ —In this case, there are quasi-steady conditions. The velocity profile spreads along the pipe at a large distance (an infinite distance for the ideal liquid).

2. $l \gg L$ —Here there is a flow rate pulsation in the pipe (Figure 7). It is an unsteady potential flow.

3. $C \sim U$ and L/l are equal to an integer value and the flow rate through the pipe is a constant. This case is more relevant for the pump operation, exhibiting vortex disturbances caused by the nonuniform flow. This is large-scale turbulence. The characteristic vortex dimension is l . According to the postulate about cascade transfer of energy from the large vortex structures to the small ones (refer to Figure 9 below), the initial vortex perturbations damp rapidly due to a turbulent energy exchange accompanied by generation of acoustic perturbations distributed further with velocity of sound. It is known that the attenuation ε of turbulence energy E does not depend on viscosity for a large-scale turbulence.

$$\varepsilon \sim C^3 / l \quad (9)$$

Thus, for the time period $T = l/U \sim l/C$:

$$\Delta E = \varepsilon T \sim C^2 \quad (10)$$

In other words, the large-scale vortices completely attenuate within the length l .

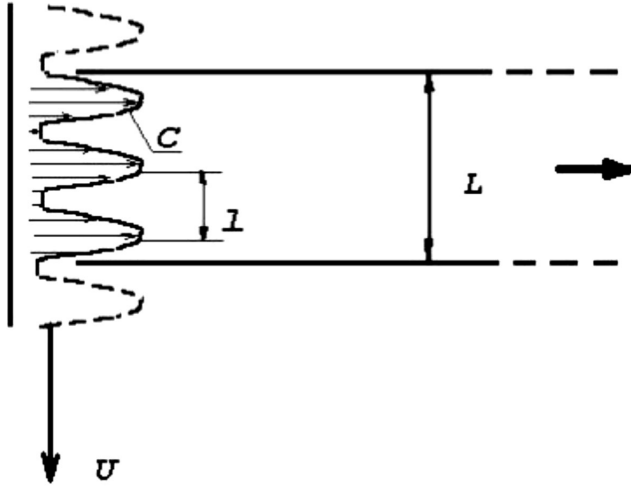


Figure 7. Simplified Model.

Near to the stator inlet the limited zone of vortex perturbations takes place. Further, in the volute and outlet pipe only acoustic waves propagate in the working fluid (Figure 8).

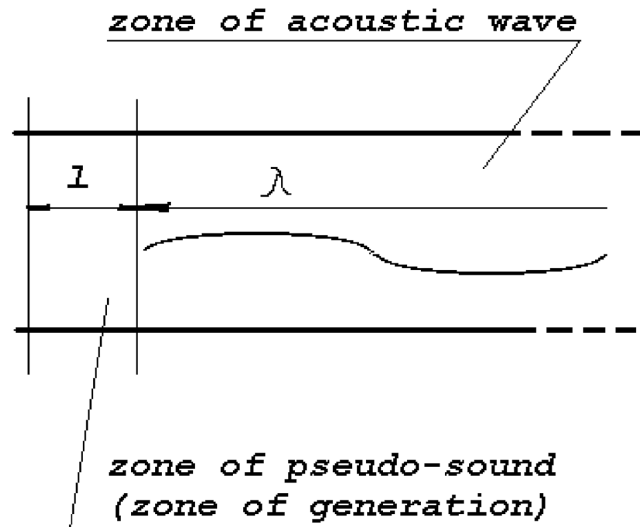


Figure 8. Zones of Pseudosound and Acoustic Wave.

The flow domain splits in two zones—zone of pseudosound with large-scale turbulence and zone of acoustic waves where large BPF vortices do not exist. Following the model (Figure 7) the acoustic wavelength:

$$\lambda = al / U \quad (11)$$

is resulting in the nondimensional criterion:

$$\Lambda = \frac{L}{\lambda} = \frac{UL}{al} = \frac{C LU}{a lC} = \frac{C Lf}{a C} = M \cdot St \quad (12)$$

Where a represents the sound speed.

Assumptions and Mathematical Model

Dissipation of vortices due to diffusion, damping of acoustic perturbations stipulated by viscosity, and the thermal phenomena have minor significance here.

There is a strict conclusion from experimental data available that to develop a mathematical model of pulsating flow in a pump:

- The nonlinear character of the generation process of oscillations and
- The acoustic nature of their distribution within the flow part of the machine needs to be taken into account.

Let us make the following assumptions:

- Subsonic flow
- Isentropic flow
- Viscous diffusion neglected
- Acoustic oscillations (velocity of acoustic motion owing to the compressibility of medium) are small in comparison with vortex oscillations (velocities of rotational and transitional motion of the fluid as an absolutely incompressible medium)

Besides, assume that the impeller flow is steady, i.e., the parameters of flow at the exit section do not depend on an angular position of the impeller. The last assumption is not a basic restriction for the applicability of the given method. Recently computational results were obtained by taking into account the influence of pump casing on impeller flow parameters.

The velocity in some points of the fluid can be determined as the sum of a velocity U transitional and rotary motion of a medium as absolutely incompressible and velocity of a pure strain V_a (Cauchy-Helmholtz theorem).

Velocity V_a represents the acoustic perturbations enabled by the compressibility of medium. Let us enter scalar function-acoustic potential ϕ . Then the acoustic velocity:

$$V_a = \nabla \phi \quad (13)$$

Thus for the fluid velocity the following expression is obtained:

$$V = U + \nabla \phi = U + V_a \quad (14)$$

The velocity of incompressible flow determines the vorticity. Let us substitute now the relation (Equation 14) in the main Euler equations of a compressible fluid. For the space scale and the characteristic velocity, take the impeller radius R_2 and impeller tip velocity u_2 . Then the dimensionless quantities of radius (r), velocity (U), time (t), and enthalpy (i) will be as follows:

$$\tilde{r} = \frac{r}{R_2}; \tilde{U} = \frac{U}{u_2}; \tilde{t} = \frac{t}{(2\pi R_2) / (u_2 z_1)}; \tilde{i} = \frac{i}{u_2^2} \quad (15)$$

Here z_1 is the number of main impeller blades. An equation of pressure oscillations (due to acoustical and vortex motion) is obtained:

$$\Lambda^2 \frac{\partial^2 h}{\partial \tau^2} - \tilde{\Delta} h = -\tilde{\Delta} g \quad (16)$$

Parameter Λ is the dimensionless similarity criterion of the given problem. A detailed derivation of Equation (16) is outlined in APPENDIX A.

It is simple to show that the parameter Λ is the product of the Mach number and the Strouhal number and represents the ratio of the impeller tip radius R_2 to the main BPF wavelength λ . It corresponds to the Ho (Helmholtz) number in classical acoustics.

$$\Lambda = \frac{u_2 z_1}{2\pi a} = \frac{f_{b1} R_2}{a} = \frac{u_2}{a} \frac{f_{b1} R_2}{u_2} = M \cdot St = \frac{R_2}{\lambda} \quad (17)$$

where:

f_{b1} = Main blade-passing frequency
 a = Speed of sound

The amplitude of pressure pulsation in a hydraulic machine is by an order of magnitude lower than the mean undisturbed pressure. Thus for enthalpy oscillations (as a sum of vortex and acoustic perturbations) it is possible to write approximately:

$$h \approx \frac{(P - P_0)}{\rho_0 u_2^2} = \frac{P'}{\rho_0 u_2^2} \quad (18)$$

where:

P = Pressure of compressible fluid
 P_0 and ρ_0 = Mean pressure and density

Similarly for oscillations of the function g , pressure pulsation ($P_v - P_0$) is obtained in "vortex-mode motion":

$$g \approx \frac{(P_v - P_0)}{\rho_0 u_2^2} = \frac{P'_v}{\rho_0 u_2^2} \quad (19)$$

Solution of Equation 16 is divided into two parts—computation of the incompressible flow for the determination of the disturbing function, and solution of the inhomogeneous wave equation for the determination of h .

The problem of pressure oscillation field determination splits into three main steps. The first one is the incompressible liquid flow analysis in the impeller to obtain unsteady boundary condition of the vortex mode flow. This boundary condition can be represented in the form of rotating velocity distribution "attached" to the impeller exit diameter. The second step is the unsteady vortex mode flow computation in the working cavity of pump or ventilator with consequential determination of the disturbance (right-part) function, and the third one is solution of the wave equation relative to pressure oscillations. The computational procedure is built on two-dimensional (2D) numerical methods. In that case, a uniform radial velocity distribution along the impeller or (equivalent) volute width is applied.

By introducing the polar coordinate system $\Theta - R$ at the pump axis and using the vorticity and streamline functions by means of the relations:

$$\Theta = \gamma \eta, R / R_2 = e^{\gamma \xi}, E = \gamma e^{\gamma \xi} \quad (20)$$

and

$$\begin{aligned} \frac{U_R}{u_2} = U_\xi = \frac{1}{E} \frac{\partial \Psi}{\partial \eta}, \quad \frac{U_\Theta}{u_2} = U_\eta = -\frac{1}{E} \frac{\partial \Psi}{\partial \xi}, \\ \zeta = \frac{1}{E} \left(\gamma U_\eta + \frac{\partial U_\eta}{\partial \xi} - \frac{\partial U_\xi}{\partial \eta} \right) \end{aligned} \quad (21)$$

The following equations are obtained:

$$\begin{aligned} \Lambda^2 \frac{\partial^2 h}{\partial \tau^2} - \frac{1}{E^2} \left(\frac{\partial^2 h}{\partial \eta^2} + \frac{\partial^2 h}{\partial \xi^2} \right) = s \\ \frac{\partial^2 \Psi}{\partial \eta^2} + \frac{\partial^2 \Psi}{\partial \xi^2} = -E^2 \zeta, \\ \frac{\partial \zeta}{\partial \tau} = -\frac{2\pi}{z_1 E} \left[\frac{\partial}{\partial \eta} (U_\eta \zeta) + \frac{\partial}{\partial \xi} (U_\xi \zeta) \right]. \end{aligned} \quad (22)$$

Boundary Conditions

Impeller Flow Analysis

Impeller flow is treated by the discrete vortex method (DVM). The DVM is used for impeller flow computation. Following recent achievements in the theory of vortex turbulent flow, DVM gives a simple and clear way of modeling large-scale or coherent structures. The important fact established is that the behavior of the large-scale turbulence does not depend on the viscosity of liquid. Large-scale characteristics of the flow can be described by Euler equations. The DVM thus becomes a very effective method for analyzing the zone of large-scale turbulence that is the cause of BPF pulsation (Figure 9).

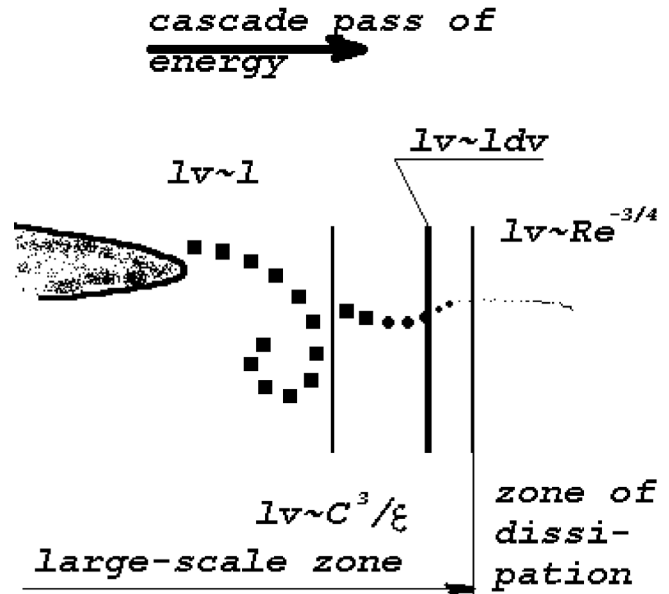


Figure 9. Cascade Pass of Turbulent Energy.

The DVM is a genuine unsteady method and it has a potential for the full simulation of turbulence, including stochastic phenomena and viscous diffusion in 3D space. The DVM gives a complete mathematical description of turbulence without additional assumptions such as k- ϵ model, etc., in 3D NS codes.

The software package has modular structure so that it is possible to use a third-party code for impeller flow computation. DVM is described in APPENDIX A.

Having the pump geometry defined, the first step in the impeller flow analysis gives an unsteady boundary condition for the solution of vortex mode equations in the form of (Ψ , ζ) equations.

Vortex Mode Flow

At the second step, the unsteady direct procedure provides a converging oscillatory solution for the incompressible liquid flow (so called "pseudosound" oscillations). In this step the following boundary conditions apply:

- On the pump volute wall:

$$\Psi_w = const, \zeta_w = 0, \quad (23)$$

- At the volute inlet boundary:

$$\Psi = \gamma \int U_{\xi} d\eta, \quad (24)$$

- At the pump casing exit:

$$\frac{\partial \Psi}{\partial n} = 0, \frac{\partial \zeta}{\partial n} = 0. \quad (25)$$

Impedance Condition for the Wave Equation

By using a local specific acoustic impedance Z (complex value), the boundary condition at the impeller outlet and pump casing exit section can be put in the form:

$$\frac{\partial (h_k - g_k)}{\partial n} = -\frac{\Lambda k}{Z_k} \frac{\partial (h_k - g_k)}{\partial \tau} \quad (26)$$

where:

k = Number of BPF harmonic

n = Normal direction to the boundary

Volute casing walls are assumed rigid. Nevertheless, there is a possibility of defining a local specific impedance of the pump housing wall that will be interesting to study the effect of damping coating.

Solution Method

The problem of pressure oscillation field determination splits into three main tasks. The first one is the incompressible liquid flow analysis in the impeller to obtain unsteady boundary condition of the vortex mode flow. The second one is the unsteady vortex mode flow computation into the working cavity of the pump with consequential determination of the disturbance function, and the third is the solution of wave equation relative to pressure oscillations, satisfying the complex specific impedance for acoustic mode and unsteady boundary condition for the pseudosound oscillations.

Application Domain

The code is applicable to centrifugal pumps or ventilators with specific speed $n_s < 150$ ($n_s = 193.3 \omega \sqrt{QH^{-3/4}}$, SI units are applied, $n_s < 2120$ using rpm, US gpm, ft) under the normal operation mode. Normal operation mode guarantees the accuracy of computation within 1 to 3 dB, based on the following conditions:

- Subsonic flow
- Homogeneous fluid
- No cavitation, operation is before the first critical mode
- Delivery range is 0.8 to 1.3 of the BEP value

Geometry may include arbitrary impeller blade profiles and arbitrary volute-diffuser geometry with one outlet pipe.

A built-in interface for the determination of impedance boundary conditions gives a possibility of taking into account the connected circuit.

Software Package and Computation Process

Numerical algorithms are realized in three main modules written in C and C++. Interface code permits an easy input of data such as impeller and casing geometry, operation mode, parameters of working fluid, acoustic impedance, and parameters controlling the computation process. It provides an environment to work with 3×3 different cases simultaneously. Once the computation procedure, which goes consequently through three main steps, finishes, it becomes possible to obtain the fluctuating pressure map in the casing at a selected time point as well as the pressure time history at any point within the working cavity with the corresponding root-mean-square (RMS) value and spectrum data.

EXAMPLES OF COMPUTATION AND EXPERIMENTAL VALIDATION

Experience shows that amplitudes of BPF pressure pulsation depend on several design factors—shape, number, and disposition of blades of the impeller and diffuser vanes, configuration of the volute, radial gap between the impeller, and volute tongue or bladed diffuser.

Due to the presence of two modes of pressure oscillation, the pump geometrical parameters can affect pressure pulsation in the pseudosound zone and in the zone of acoustic oscillations. For example, a change of radial gap influences vortex (pseudosound) fluctuations and acoustic pulsations as the radial gap is located in the zone of pseudosound, i.e., in the source of acoustic waves.

Amplification of pressure pulsation can happen due to matching of frequencies of oscillations with acoustic resonance frequencies of both the outlet duct and the pump casing flow cavity. The specific resonance phenomena often take place due to interaction between acoustic waves emitted from different vane channels with different phases defined by relation of impeller blades and diffuser vanes. Therefore, the variation of rotational speed, number of impeller blades, and diffuser vanes can substantially modify the amplitudes of pressure pulsation due to the resonance in the pump cavity. All these topics can be the subject of a computational study with the numerical method developed. Possible tasks that can be solved with the method are outlined below.

- Pressure pulsations in various points of a pump volute casing and diffuser
- Influence of flow rate
- Influence of rotation speed
- Influence of radial gap
- Influence of geometry of the impeller (number and shape of blades, intermediary short blades, arbitrary number of blade rows)
- Influence of a pump casing geometry
- Effect of damping coating
- Effect of the outlet duct impedance
- Influence of geometry of the bladed diffuser
- Determination of unsteady loads acting on impeller and diffuser blades
- Determination of diagnostics' signs such as breakage of impeller blade

In Table 1, one can see a few computational estimations of the influence of various factors on pressure pulsation amplitude.

Table 1. Various Factors Influencing Pressure Pulsation.

Factor	Rough estimation of influence (dB)
Position in the pump working cavity	15
Radial gap change from 4% to 7% (no resonance case)	6
Increasing rotation speed by 20% (no resonance case)	3
Specific impeller geometry change (no resonance case)	9
Relation of numbers of impeller and diffuser blades (resonance)	20
Damping coating in the conical diffuser	8
Outlet pipe acoustic impedance (resonance)	15

Validation Using Experimental Centrifugal Pump

A centrifugal experimental air pump (Tourret, et al., 1991) was used for validation of the numerical method. The experimental pump was tested with rotation speed of 1400 rpm and flow rate $0.0139 \text{ m}^3/\text{s}$ ($0.0456 \text{ ft}^3/\text{s}$). There are more than 300 measurement points of pressure pulsation located in the volute and at the pump exit.

In the computational procedure, the unsteady boundary condition was obtained as a stationary velocity profile at the impeller exit that rotates with the impeller. This case corresponds

to symmetrical impeller flow when the impeller is considered without volute and discharging into an infinite medium. Distribution of relative velocity (reduced by impeller tip velocity) in impeller channels (Figure 10) shows low-velocity zones near the suction side of each blade.

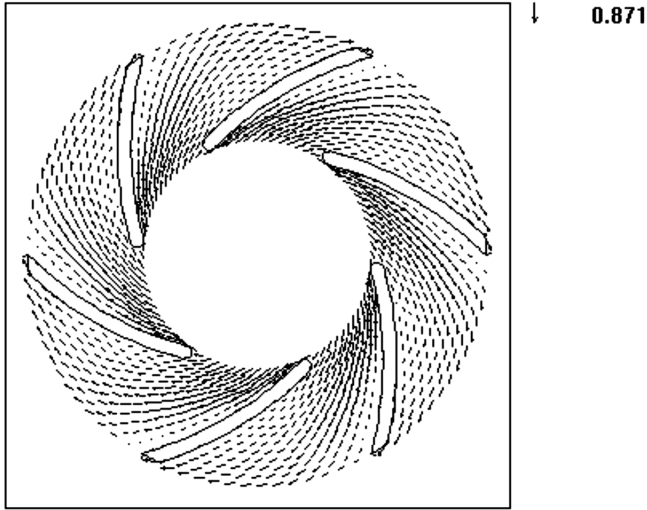


Figure 10. Relative Velocity in Impeller Channels.

This leads to the nonuniform distribution of flow parameters at the impeller exit that are presented in Figure 11 and Figure 12. In these figures, the pressure side of the blade channel is on the left, while the impeller rotation goes to the right. Thus, the maximum of radial velocity and minimum of absolute tangential velocity are located near the pressure side of the blade.

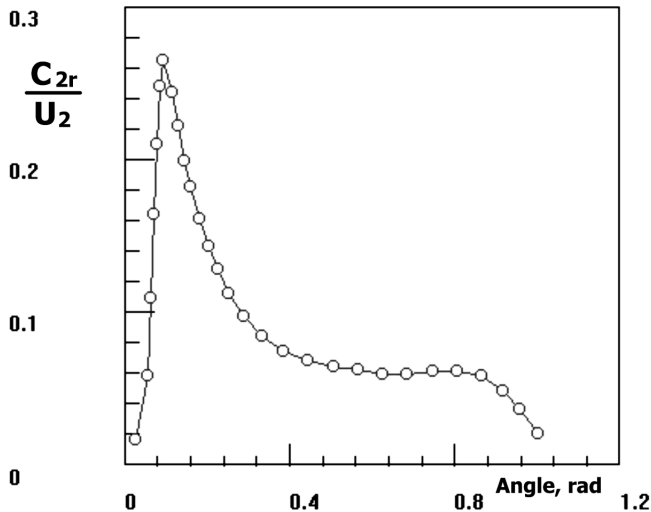


Figure 11. Absolute Radial Velocity along the Impeller Channel Span at the Impeller Exit.

With more than 10,000 overall mesh nodes (number of mesh nodes in impeller channel span is 12), total computation time on a Pentium® II processor is six hours. Seven BPF harmonics are included for the computation of pressure pulsation. The pump has no exit pipe, thus a computation open-end-condition is taken for the acoustic mode.

The characteristic feature of unsteady pressure in the pump volute is the presence of lower pressure zones linked with blade exit edges and rotating with the impeller. Computation also shows such zones (Figure 13). For comparison, Figure 14 presents the experimental oscillatory part of the static pressure field.

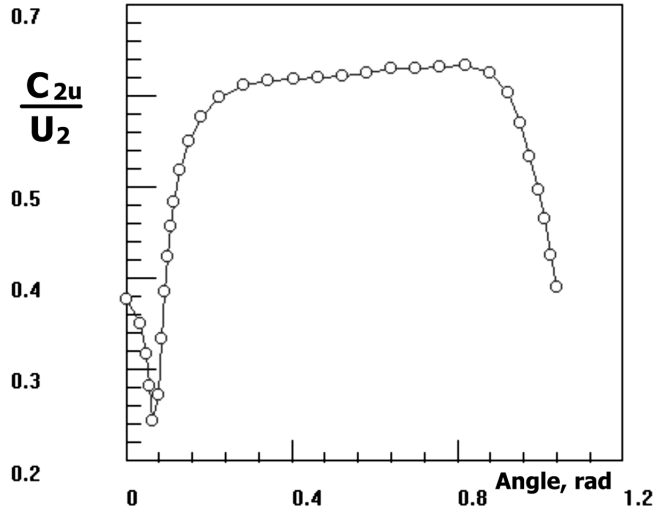


Figure 12. Absolute Tangential Velocity along the Impeller Channel Span at the Impeller Exit.

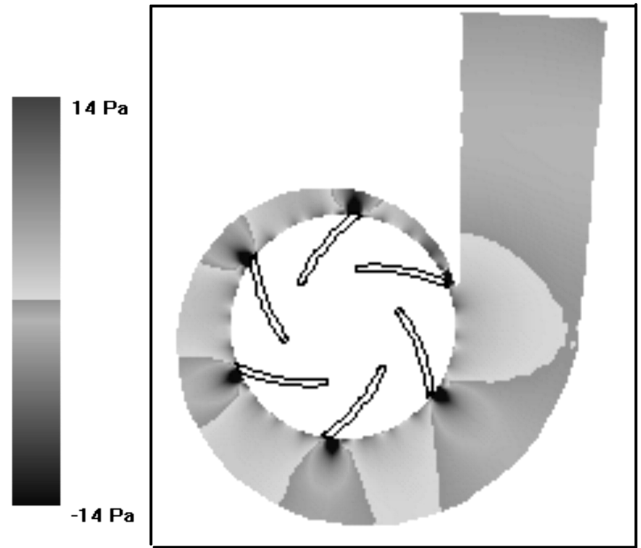


Figure 13. Unsteady Pressure Map in the Volute (Computation for Seven Harmonics of BPF); Grayscale Palette from -14Pa to +14Pa.

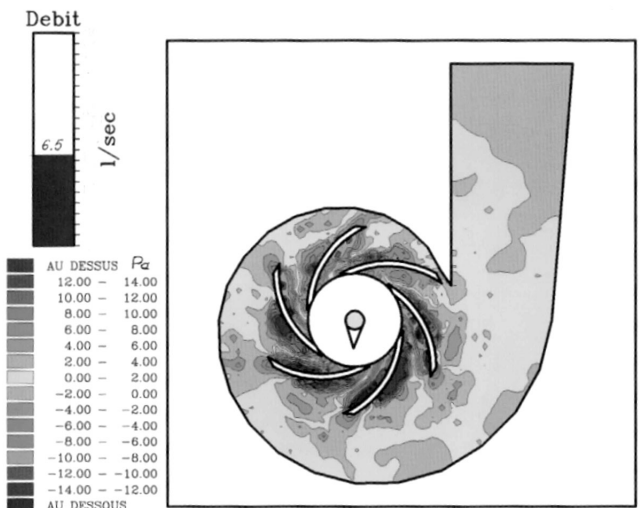


Figure 14. Unsteady Pressure Map (Experiment, Lower Flow Rate).

In the spectrum, there are three main harmonics of blade-passing frequency. In Figure 15 and Figure 16 there are a comparison of amplitude maps (computed and measured) for the first harmonic of blade-passing frequency. Furthermore, the pressure amplitudes stand in good agreement with the experimental data. The mismatch is mostly below 3 dB.

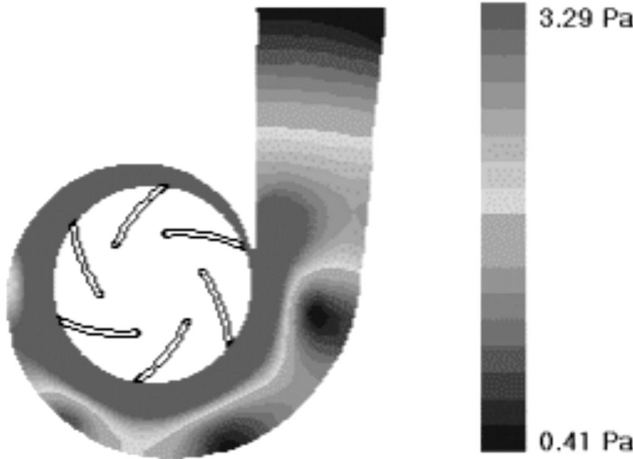


Figure 15. Map of the First Harmonic Amplitude (Computation).

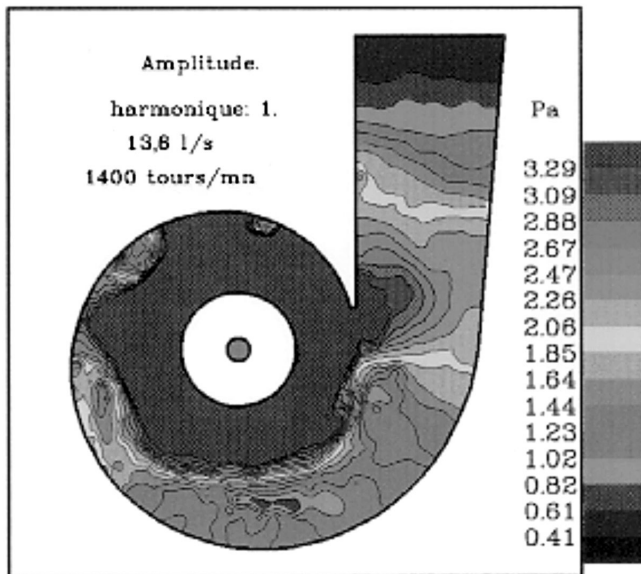


Figure 16. Map of the First Harmonic Amplitude (Experiment).

Such agreement in amplitude map gives a possibility of obtaining both the right amplitude and also the shape of the pressure signal. In Figure 17 and Figure 18, the computed and measured signals of pressure pulsation at a point in the volute are shown. The open-end-condition at the diffuser exit enforces pressure pulsation amplification on the third harmonic of blade-passing frequency.

Exit Impedance Effect—Computational Prediction

The study case corresponds to the actual geometry of the experimental pump discussed above. The same pump was computed for open-end and infinite-pipe exit condition to determine the exit impedance effect on pressure pulsation within the pump working cavity. It was found that in the major part of the volute the exit impedance practically does not affect pulsation amplitude. Near the throat of the volute, pulsation has almost the same amplitude but a different shape, as can be seen in Figure 19.

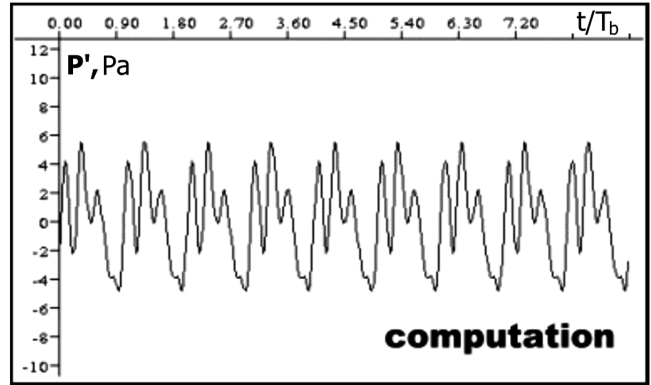


Figure 17. Pressure Pulsations in the Volute Throat [Pa] (Computation).

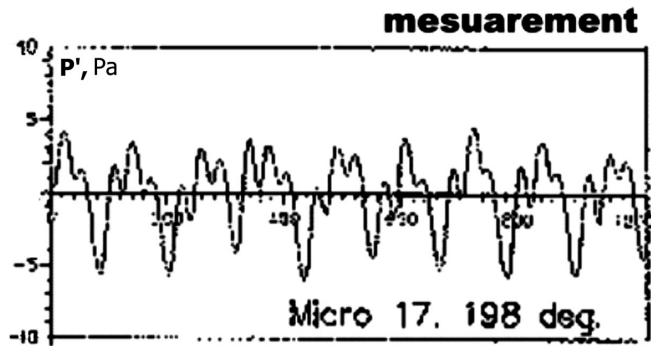


Figure 18. Pressure Pulsations in the Volute Throat [Pa] (Experiment).

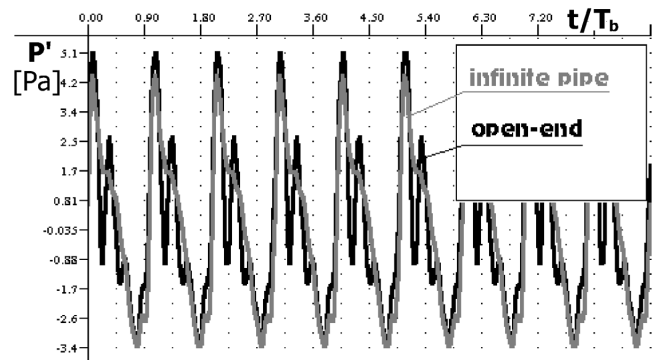


Figure 19. Computed Pressure Pulsation in the Volute Throat Section of Pump.

The biggest difference between these cases was found certainly at the pump exit (Figure 20) and outlet pipe where there is a considerable difference both in amplitude and in the shape of signal.

Incorporation of the Influence of the Volute on Impeller Flow Computation

The distribution of impeller flow velocity along the impeller exit is represented in absolute reference frame. Absolute velocity distribution is obtained in 72 equidistant angular (every five degrees) points on the radius $1.018 R_2$. Volute tongue edge angular position is referenced as zero degrees.

The point at zero degrees is named “1” on velocity distribution plots. Point numbers increase in counterclockwise direction. Point 72 is just slightly (five degrees) before the tongue.

After each turn of the impeller, Fourier harmonic analysis was performed to define mean value and amplitudes of radial and

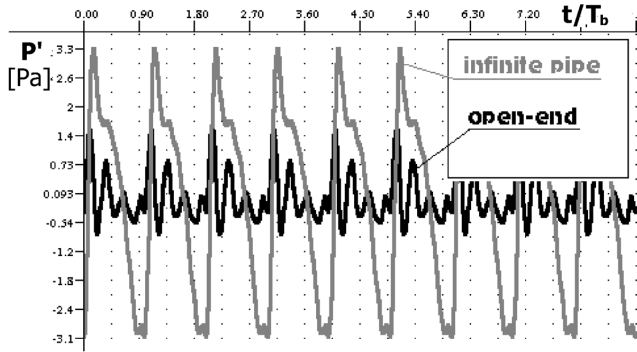


Figure 20. Computed Pressure Pulsation at the Pump Exit.

tangential components of absolute velocity. Blade passage period was taken as the main period of Fourier analysis.

The numerical procedure described in the previous section uses symmetrical impeller flow analysis and does not take into account the influence of the stator on impeller flow parameters. It is not a strict limitation. A new method has been developed to study this phenomenon. In this section computational results are presented for the same experimental pump described in the previous section. The code gives an unsteady behavior of the impeller flow. On the initial stage of impeller rotation, it is possible to see formation of starting vortices in each channel (Figure 21).

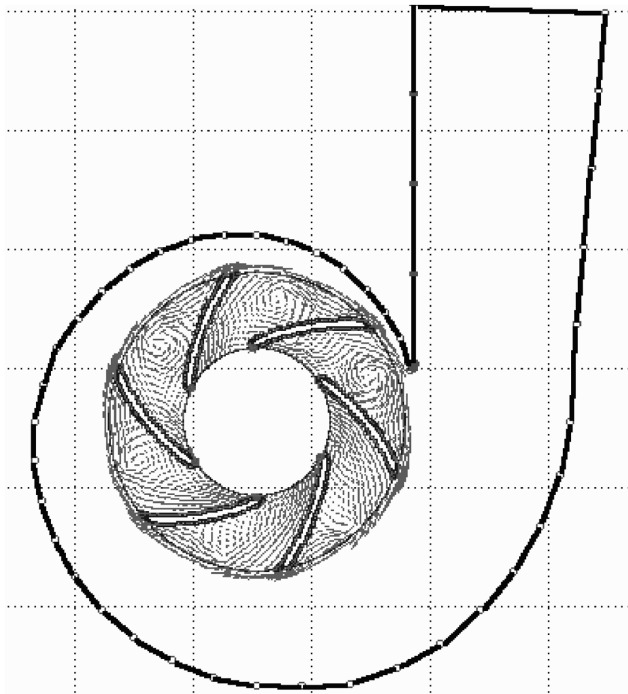


Figure 21. Starting Vortices in Impeller Channels.

A bit later there is a gradual damping of starting vortices, however the flow in the impeller continues to be asymmetrical. It was found that a spatial perturbation of velocity distribution was caused by the initial flow condition, and convergence improved after six to eight impeller turns. The main goal is to study the unsteady velocity and pressure in impeller channels caused by the influence of volute casing or bladed diffuser on impeller flow parameters. It gives a more accurate prediction of pseudosound oscillation near the volute tongue (or diffuser blade) and unsteady load acting on impeller blades and the rotor. Computational data include 10 impeller turns after starting its rotation.

Mean Velocities

General features of mean velocity distributions follow. Near the volute tongue edge radial velocity has the absolute minimum. Just after the tongue, in the beginning of the volute, there is an absolute maximum of radial velocity within angle range from zero degrees to 25 degrees.

Contrarily, tangential velocity has an absolute maximum near the tongue edge and goes to minimal value after 30 degrees. These features of velocity distribution are established straight away, after the first impeller turn.

At the same time, there is a big spatial perturbation of velocity distribution. After the first impeller turn peaks of radial and tangential velocity appear at 140 degrees to 60 degrees angular position. Then this perturbation slowly shifts to lower angular positions with attenuation of (spatial) amplitude. It can be seen in Figure 22 and Figure 23 that after six turns of the impeller there is a close convergence of the mean velocity distribution, although there is a tendency of subsequent attenuation of initial spatial perturbation.

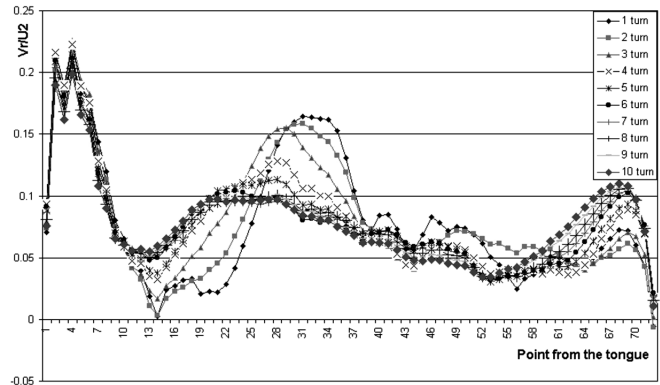


Figure 22. Mean Value of Radial Velocity; Impeller with Volute.

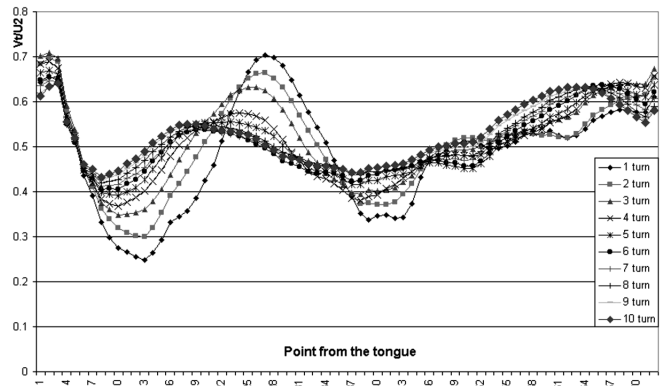


Figure 23. Mean Value of Tangential Velocity; Impeller with Volute.

Velocity Oscillation

Velocity oscillation data were obtained as nine harmonics of blade-passing frequency. Amplitudes of the first BPF harmonic of radial and tangential velocity are presented in Figure 24 and Figure 25. It could be proved from these data that after six impeller turns there is definitive convergence in spatial distribution of amplitude values. They have local maximum near the tongue edge, absolute minimum at 20 degrees and local maximum at 60 degrees.

The mean value of tangential velocity under volute presence is less than for axisymmetrical computation. The same must be indicated about the amplitude of tangential velocity fluctuation.

BPF Pressure Pulsation

BPF pressure pulsation was computed on the same polar grid as in the previous computational test but using the new boundary

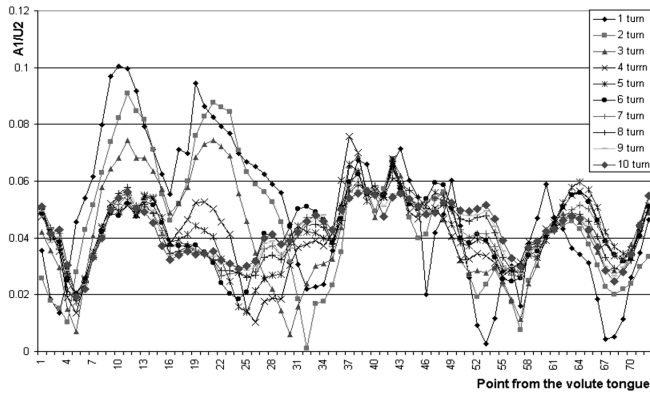


Figure 24. Amplitude of the First Harmonic of Radial Velocity.

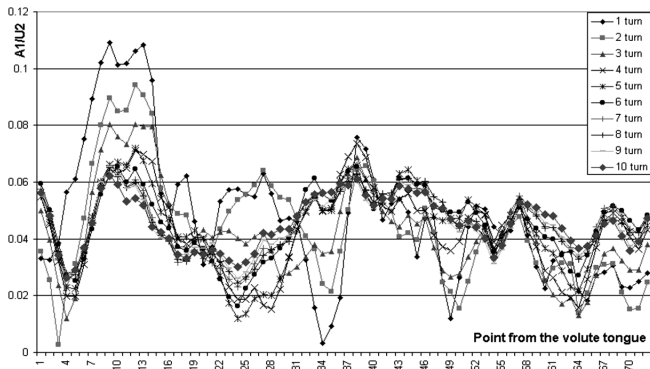


Figure 25. Amplitude of the First Harmonic of Tangential Velocity.

condition procedure. Unsteady boundary condition for the vortex mode flow is defined from Fourier coefficients of impeller flow parameters. Computed signals of pressure pulsation were compared with experimental data. Location of pressure sensors in an experimental air pump is shown in Figure 26.

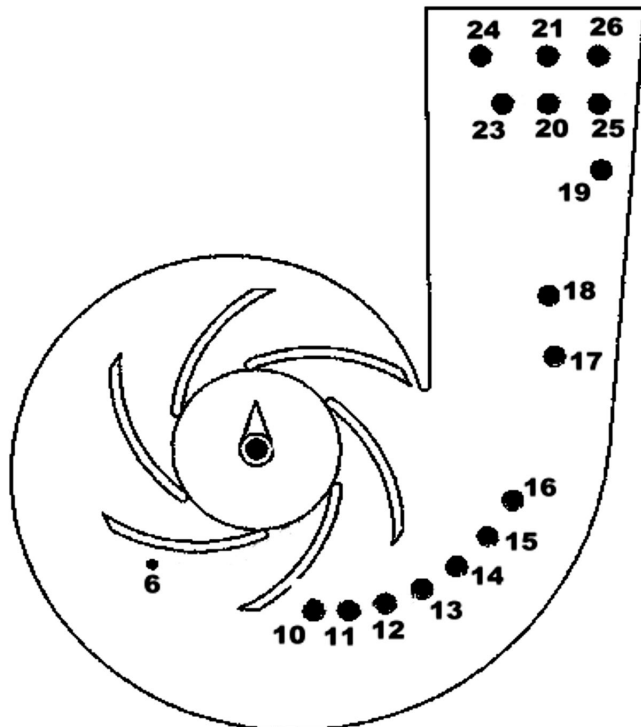


Figure 26. Installation of Pressure Sensors in Experimental Pump.

Pressure signals for different points indicated in Figure 26 are compared for the version MK1 (symmetrical impeller flow in infinite medium) and MK3 (impeller with volute).

Total amplitude of computed signal (MK3 versus MK1) was compared with experimental data as it is shown in Figure 27. Experimental amplitudes are represented by minimal (MIN) and maximal (MAX) values. The difference between min and max values shows some instability in the amplitude of experimental signals. Version MK3 improves prediction of pressure pulsation amplitude near impeller exit (sensors 6 and 10) by approximately 6 dB. This is important for improving the prediction accuracy of the unsteady loads acting on the tongue, diffuser vanes, and impeller blades. At the same time, one can see that prediction of version MK1 is valuable for the rest of the pump flow part.

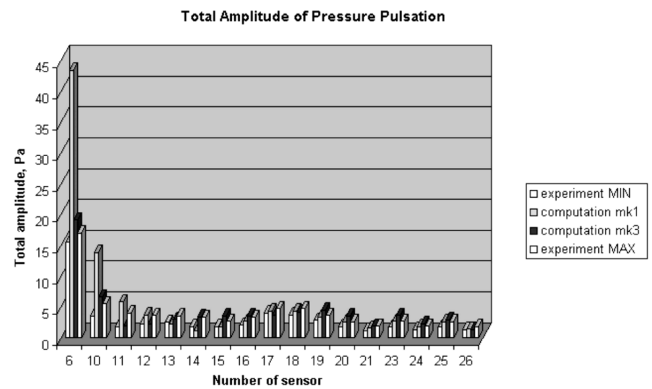


Figure 27. Comparison of Computational Data with Experiment.

Computational Prediction of Diagnostic Sign of Impeller Breakage

In all steps of version MK3 computation, direct numerical procedures will be used. So, the pressure pulsation field can be obtained at each time point. It is possible to simulate the really unsteady behavior of flow due to a change in pump geometry and/or operation mode. One will be able to predict, for example, important signs of pump breakage by computational experiments and gain indicators for a diagnostic maintenance system. Another possibility is to find steady oscillatory conditions corresponding to different stages of the impeller deterioration. In the study presented below three cases are computed for a pump with an impeller having six blades.

One of the blades gets some deterioration of the inlet edge. Computation is completed for six harmonics of the rotor frequency. It can be seen in Figure 28 that initial deterioration brings an increase of the amplitude of the second harmonic of rotor frequency in pressure pulsation signal at the pump exit. With extending of a deterioration the first harmonic of rotor-frequency becomes dominant.

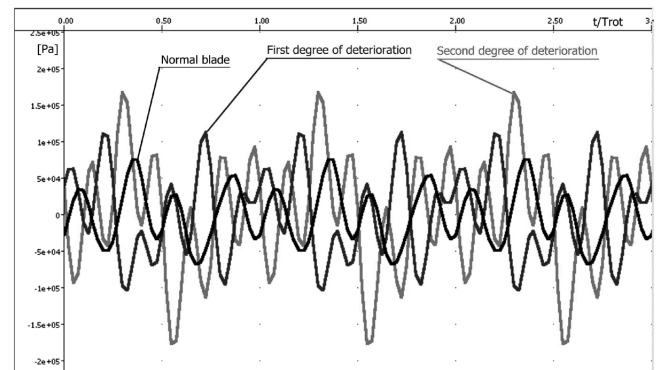


Figure 28. Pulsation of Pressure at the Pump Exit.

Radial Gap Effect—Comparison with Experimental Data

Radial gap is expressed by Equation (3). Computational study of radial gap effect was performed for an industrial-type centrifugal pump tested with measurements of pressure pulsation. The pump has an impeller outlet radius of 173 mm (6.8 in) with five blades. The BEP operation mode case of 1200 rpm, $Q = 0.066 \text{ m}^3/\text{s}$ ($0.2165 \text{ ft}^3/\text{s}$) was computed; exit impedance condition was “infinite-pipe.”

The study covered four volutes with radial gaps of 2, 7 (actual pump geometry), 11, and 18 percent. The radial gap change was made without impairing the rest of the pump geometry. All geometry parameters of the conical diffuser and tongue were kept unchanged (Figure 29). Therefore, the result presents a “pure” effect of the radial gap on pressure pulsation.

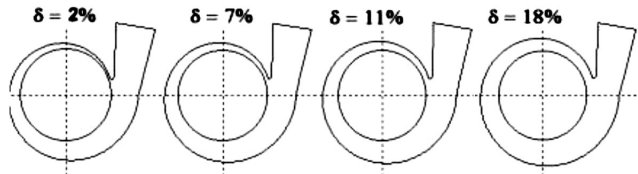


Figure 29. Pump Geometry for Different Radial Gaps.

The numerical dimensionless amplitude of the total signal (four BPF harmonics included) defined with the formula:

$$\bar{A} = A / \left(\frac{1}{2} \rho \cdot U_2^2 \right) \quad (27)$$

was derived for two points—pump exit and lower edge of tongue, and then compared (Figure 30) with experimental data published by Zogg and Bolleter (1993).

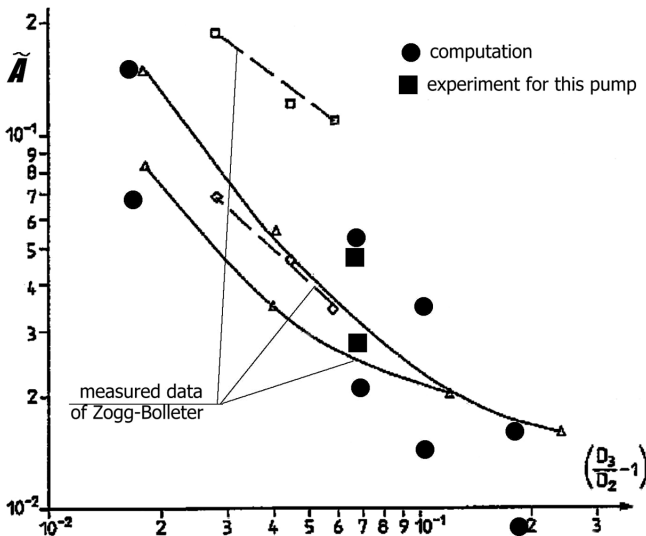


Figure 30. Influence of a Radial Gap on Total Amplitude of Pressure Pulsation.

The experimental data suggest the possibility of predicting an absolute effect of the radial gap change. These data show that there is a considerable difference in pressure pulsation amplitudes in a pump cavity—the upper level computed relates to the volute tongue point.

Computational Data on Influence of Radial Gap Change

A computational study was performed for the same industrial water pump described in the previous section, which included three volutes (Figure 31): case 1 with a radial gap of 7 percent (actual pump geometry) and cases 2 and 3 with a radial gap of 11

percent. In case 2, the radial gap change was made without affecting the rest of the pump geometry; all geometry parameters of the conical diffuser and the tongue were kept unchanged. In case 3 the same increase of the radial gap was reached by cutting the tongue.

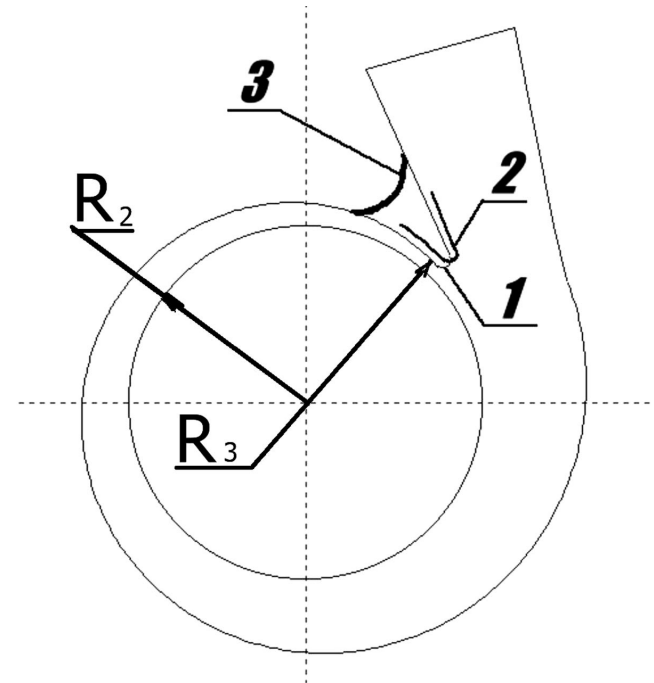


Figure 31. Increasing of Radial Gap (1 - 7 Percent, 2 - 11 Percent, 3 - Cut to 11 Percent).

In Figure 32 computed dimensionless amplitudes of total signal (four BPF harmonics included) are presented. It can be seen that the tongue cut is a more effective method for amplitude reduction, but in case (3), the shape of the signal essentially changes with increase of the second BPF harmonic.

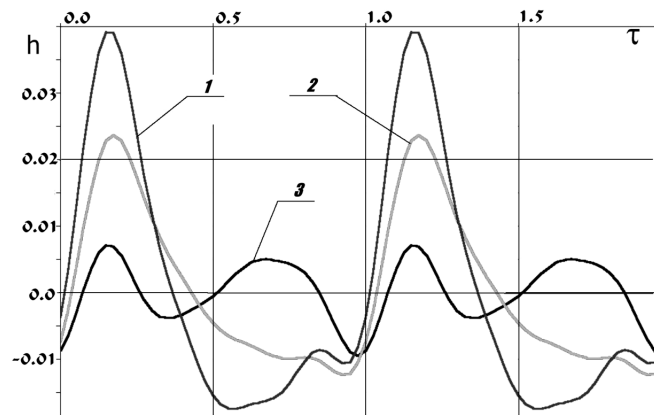


Figure 32. Reduced Pressure Pulsation “h” on the Volute Tongue (1 - 7 Percent, 2 - 11 Percent, 3 - Cut to 11 Percent).

Unsteady Loads Acting on Impeller Blades

Using the MK3 method, one is able to compute unsteady loads acting on impeller blades in the industrial water pump described in previous sections. They are obtained by a direct unsteady computation of static pressure field. The data outlined concern tenth impeller turn. In Figure 33 the instantaneous distribution of blade load is presented at the instant when one impeller blade is passing the volute tongue. The load is maximal for that blade.

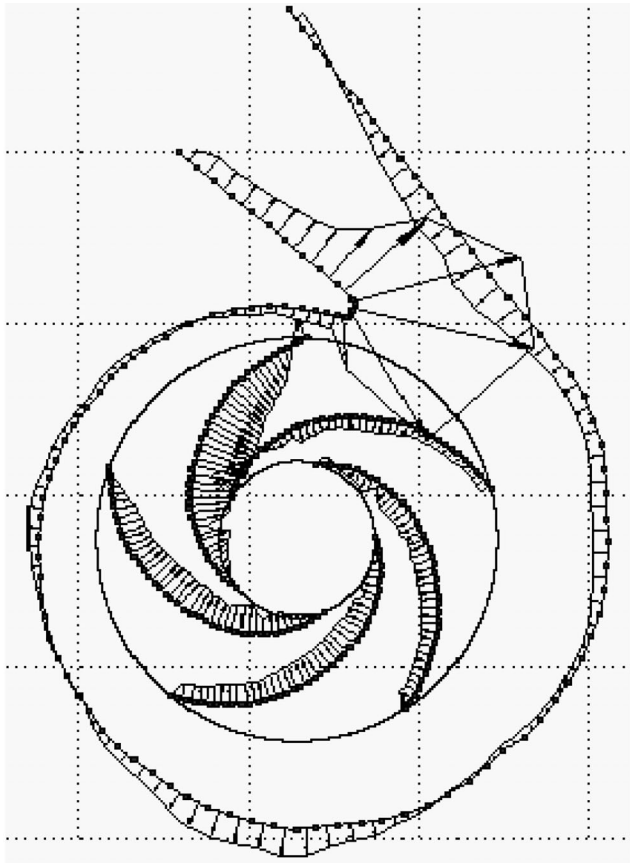


Figure 33. Unsteady Loads Acting on Impeller Blades.

In Figure 33 the load acting on the volute casing is shown as well, but these data have only qualitative significance as the current version of the DVM method has no possibility of accurately calculating loads acting on the casing of pump.

Time curves of radial and tangential forces acting on different blades are presented in Figure 34 and Figure 35. A minus sign shows that these forces act against a positive direction of velocities. It can be stated that the radial and tangential force has a maximum when a blade is passing the volute tongue.

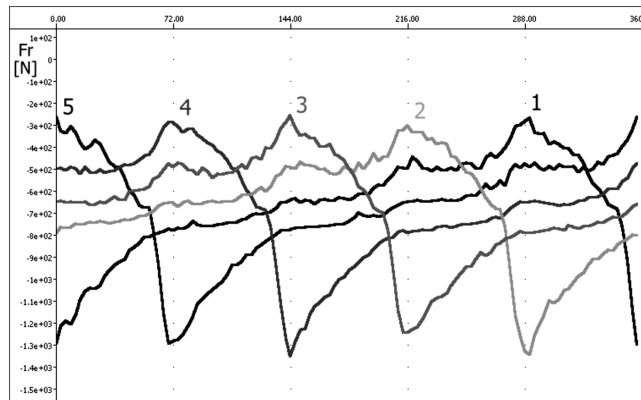


Figure 34. Radial Load Acting on Different Impeller Blades.

The next blade has a minimal load at that moment. Behavior of the radial and tangential force is similar but amplitudes differ. Radial force changes from 300 N to 1300 N and tangential force changes from 120 N to 600 N. With such data, it is possible to estimate the pump power and vibration of the rotor due to hydraulic forces.

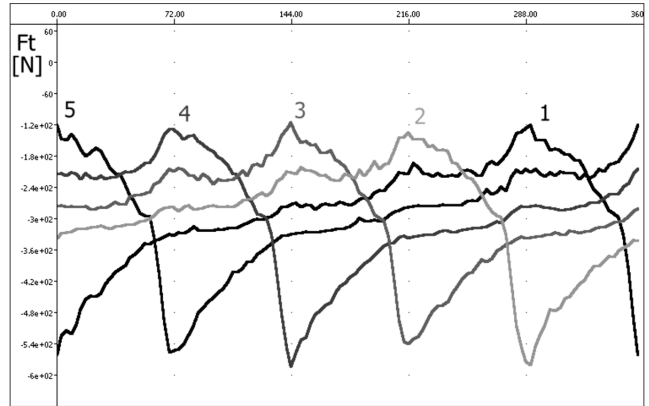


Figure 35. Tangential Load Acting on Different Impeller Blades.

Effect of Impeller Geometry Change—Computational Prediction

Influence of intermediary short blades was computationally studied on the base of a new pump under development. Six types of impeller geometry include five long blades (impeller 3), five long and five short blades positioned axisymmetrically at the impeller exit (impeller 4), the same number of long and short blades but positioned nonaxisymmetrically at the impeller exit (impeller 5), and other types with the same number of blades (impeller 6, 7, and 8). All computations were completed for the same pump casing of 30 percent radial gap and the same operation parameters. “Infinite-pipe” condition was defined at the pump exit.

Impeller Geometry Change

The effect of Coriolis forces and secondary flows on parameters of flow in a blade channel of a centrifugal impeller is distributed nonuniformly. Along the angle coordinate the relative velocity and flow angle are higher near the pressure side of the blade channel. Near the suction side of the blade the low energy zone is formed. The task was to act on the low energy zone of flow with intermediary shortened blades.

For better understanding of the impeller geometry change, Figure 36 shows consecutive changes in geometry by adding different intermediary profiles to the long profile 3. The inlet edge of the short blade penetrates into the low energy zone. The exit blade angle is altered as well to obtain a more optimal result. Profile 7 gave the best result in reduction of BPF pressure pulsation. Profile 3 of the long blade was unchanged for all cases computed.

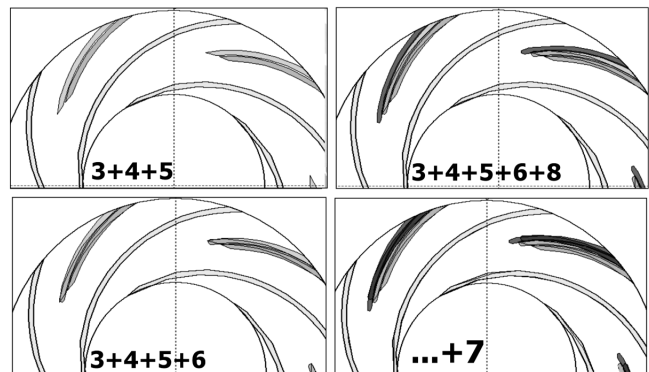


Figure 36. Change of Impeller Geometry by Adding Splitters.

Distribution of Flow Parameters along the Blade Channel Span

Distributions of radial and tangential velocity components along the blade span between two long blades shows a considerable

change of nonuniformity of flow. Additional blades give an additional peak in the velocity distribution. For profile 7 two peaks are approximately equal, which gives more balanced flow delivery at the impeller exit. Besides, this gives a rise of impeller head of 20 percent.

It is found that nonuniformity of the distribution of tangential velocity component was reduced due to influence of intermediary blades.

The initial negative peak in vorticity distribution was split into two approximately equal parts. For profile 7 these parts are more balanced in value and space—one peak being situated in the middle of the main channel.

Pressure Pulsation

Analysis of the amplitude distribution of the first BPF harmonic shows that all impellers with intermediary blades give reduction of amplitude. For impeller geometry 7 it looks like a complete elimination of the first harmonic. This result shows the importance of providing specific impeller geometry to achieve a desired pressure pulsation spectrum.

It can be seen that the level of amplitude of the second harmonic for all geometry types undergoing study is comparable due to the presence of two peaks of vorticity in impellers with intermediary blades. This brings some amplitude rise at the pump exit. However, the level of amplitude is smaller than for the first harmonic. Therefore, total amplitude of BPF pressure pulsation is reduced. Dimensionless pressure pulsation signal at the pump exit (Figure 37) shows a considerable change in amplitude as well as in shape of signal. Intermediary blades give a relative rise of the second BPF harmonic but the total amplitude is lower.

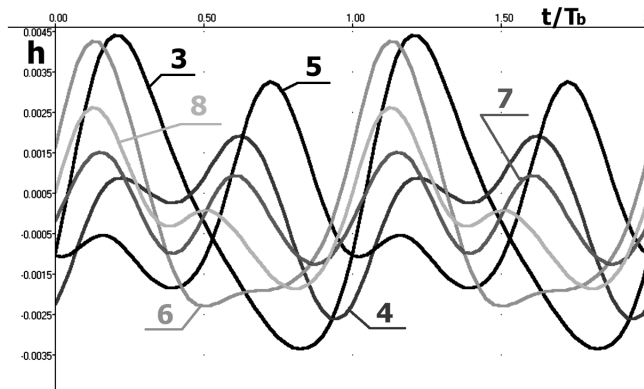


Figure 37. Reduced Pressure Pulsation “h” at the Pump Exit.

Regarding the reduction of pressure pulsation, profile 7 must be indicated as a very good perspective to reduce pressure pulsation at the main BPF frequency and total amplitude of pressure pulsation into the pump cavity and in the outlet pipe. It reduces total amplitude by a factor of three.

This study demonstrates the main advantage of the software package to rapidly provide computational experiments in the early stage of design in order to select the right direction of the whole development project without experimental costs.

Computational Data on the Effect of Helmholtz Number

The Helmholtz number is represented in acoustic-vortex equation by parameter Λ . Figure 38, Figure 39, and Figure 40 show the distribution of amplitude of the first harmonic of BPF in the air experimental pump and two types of ventilators. All machines have a simple volute design, but parameter Λ differs considerably. Besides, in the ventilators the relative size of vortex perturbations is much less because of the many blades of the centrifugal impeller. In the last case (Figure 40) the transverse dimension of the volute is comparable with the impeller diameter. The light zone in the

grayscale pictures divides domains with low (“L”) and high (“H”) amplitudes. At small Λ (air pump), pressure oscillations in a considerable part of the volute are formed by pseudosound oscillations having high amplitude. Low-amplitude zone at the pump exit (Figure 38) is obtained due to the effect of “open-end-condition.”

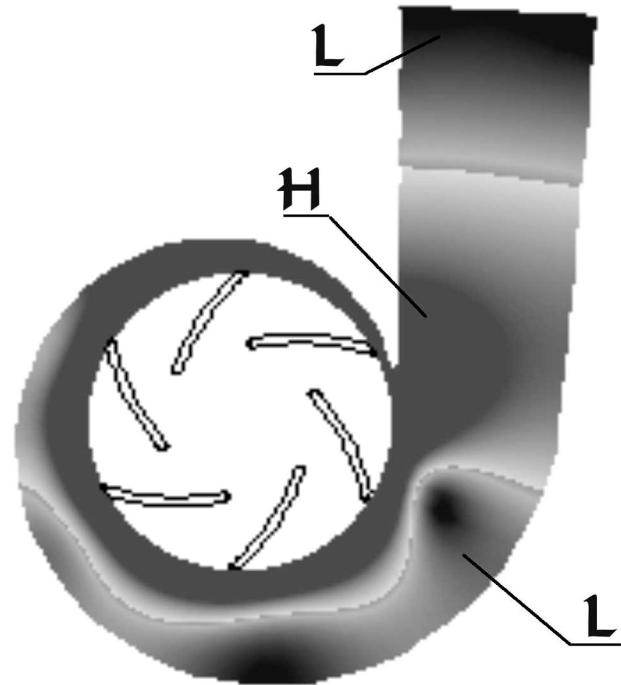


Figure 38. Distribution of the First BPF Amplitude; Simple Volute; $\Lambda = 0.04$.

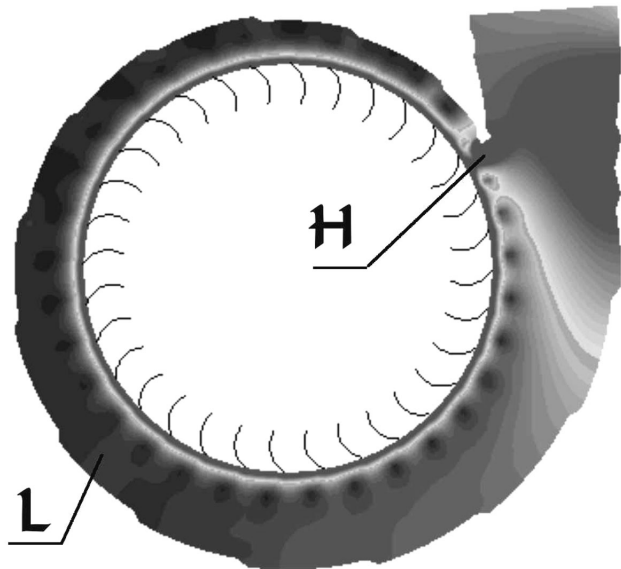


Figure 39. Distribution of the First BPF Amplitude; Simple Volute; $\Lambda = 0.37$.

In the ventilators, the zone of high amplitudes is fixed only in immediate proximity to the impeller exit, and the remaining part of the volute is occupied by acoustic waves. “Infinite-pipe-condition” is applied at the exit cross-section for both ventilators.

In the last case (Figure 40), one can see two low-amplitude (“node”) zones in the volute. It shows that transverse mode of acoustical pressure pulsation occurs in this volute.

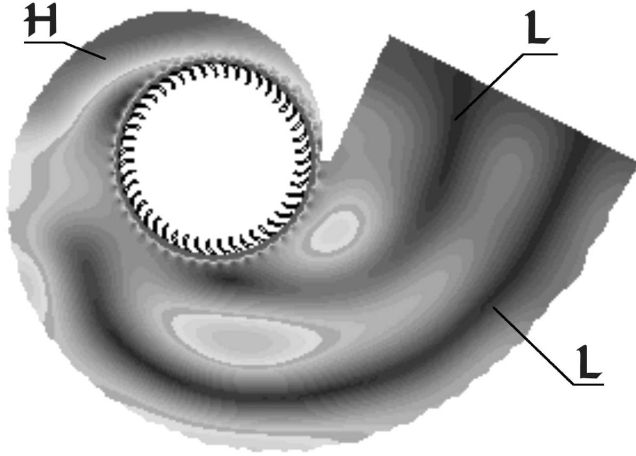


Figure 40. Distribution of the First BPF Amplitude; Simple Volute; $\Lambda = 0.48$.

Computation of air pump model with bladed diffuser has been undertaken by using curvilinear 2D coordinate system. "Infinite-pipe-condition" was applied at the pump exit. The results are shown in Figure 41. Although $\Lambda = 0.14$ in this case, the pressure pulsation field is produced by interaction of acoustic waves outgoing from different channels of the bladed diffuser. Due to amplification effect, maximal amplitude is found within the volute and outlet part of the bladed diffuser.

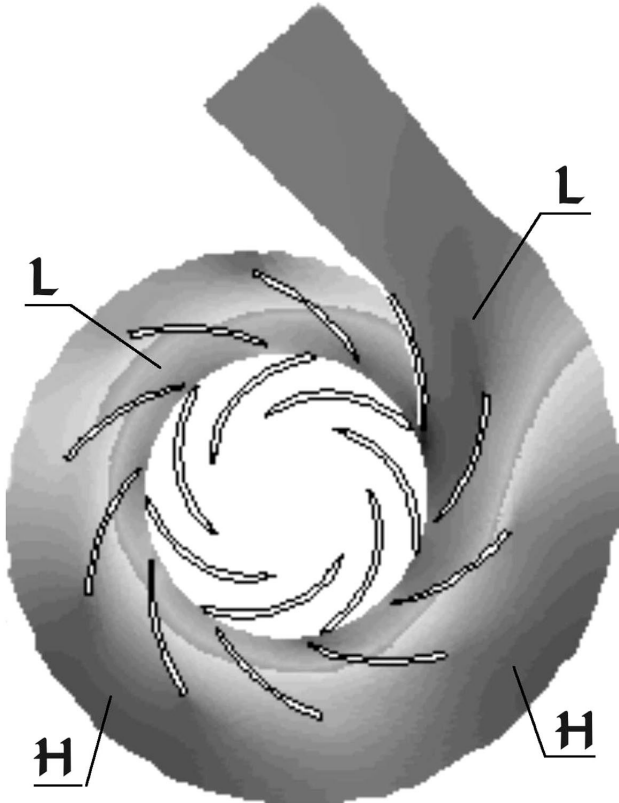


Figure 41. Distribution of the First BPF Amplitude; Bladed Diffuser; $\Lambda = 0.14$.

CONCLUSIONS

- Distribution of BPF pressure pulsation amplitude within the volute casing of a centrifugal pump (ventilator) depends on criterion Λ (relation of impeller tip radius to the main BPF wave

length) and volute transverse dimension. In a pump with bladed diffuser, maximal amplitudes of BPF pressure pulsation can occur in the volute due to acoustical resonance.

- With the same radial gap the amplitude and shape of pressure pulsation signal depend on the thickness of volute tongue.
- Numerical method taking into account the influence of the pump casing on impeller flow improves the prediction accuracy of pressure pulsation near the impeller exit. It is possible to compute unsteady blade loads, unsteady momentum (power), and hydraulic vibration of the rotor. Prediction of pressure pulsation based on the axisymmetrical impeller flow data is valuable for the rest of the pump flow passage.
- Impeller with additional shortened blades gives reduction of BPF pressure pulsation and increase of pump head by 20 percent against the same impeller without shortened blades.
- Computational study shows that the initial deterioration of the inlet edge of one impeller blade causes an increase of the second harmonic of rotor frequency in pressure pulsation signal.

APPENDIX A

Main Equations

Omitting appropriate terms due to above-mentioned assumptions, main equations of motion of a compressible medium are as follows:

$$\frac{\partial V}{\partial t} + \nabla \frac{V^2}{2} - V \times (\nabla \times V) = -\frac{\nabla P}{\rho} \quad (\text{A-1})$$

$$\frac{\partial \rho}{\partial t} + \nabla(\rho V) = 0 \quad (\text{A-2})$$

$$s = \text{const} \quad (\text{A-3})$$

The mathematical model is based on a representation of fluctuating flow velocity V as a combination of vortex and acoustic modes,

$$V = U + \nabla \varphi = U + V_a \quad (\text{A-4})$$

where:

U = Velocity of translational and rotational motion of incompressible liquid (vortex mode)

V_a = Velocity of pure deformation (acoustic mode)

φ = Acoustic potential

Thus the velocity of incompressible flow determines the vorticity. Let us substitute now Equation (A-4) in the main equations. After a few transformations the equation results in:

$$\frac{1}{a^2} \frac{d^2 \varphi}{dt^2} - \Delta \varphi = \frac{1}{a^2} \frac{dj}{dt} \quad (\text{A-5})$$

The disturbing function in the right term of Equation (A-5) can be expressed through a velocity field of flow of incompressible fluid (vortex mode):

$$-\Delta j = \nabla(U \nabla U) = \nabla \left(\nabla \left(\frac{1}{2} U^2 \right) - U \times \zeta \right) \quad (\text{A-6})$$

Upon transferring the convective term in the time derivative to the right side of Equation (A-5) we get:

$$\frac{1}{a^2} \frac{d^2 i}{dt^2} - \Delta i = -\Delta j \quad (\text{A-7})$$

where S designates the disturbing function, defined from the field of velocities of vortex mode flow:

$$-\Delta j = \nabla(U \nabla U) = \nabla \left(\nabla \left(\frac{1}{2} U^2 \right) - U \times \zeta \right) \quad (\text{A-8})$$

and K the convective term:

$$K = 2U\nabla\left(\frac{di}{dt}\right) + (U\nabla)(U\nabla i) \quad (\text{A-9})$$

Let us proceed now to dimensionless variables. For the space scale and the characteristic velocity we shall take the pitch of working cascade l_2 and the peripheral velocity u_2 at the exit diameter of the impeller. Then the dimensionless quantities are as follows:

$$\tilde{x} = \frac{x}{l_2}; \tilde{U} = \frac{U}{u_2}; \tilde{t} = \frac{t}{l_2/u_2}; \tilde{i} = \frac{i}{u_2^2} \quad (\text{A-10})$$

Substituting Equation (A-10) into the Equation (A-7), we get:

$$\Lambda^2 \frac{\partial^2 \tilde{i}}{\partial \tilde{t}^2} - \tilde{\Delta} \tilde{i} = \tilde{S} - \Lambda^2 \tilde{K} \quad (\text{A-11})$$

Parameter $\Lambda = \frac{u_2}{a}$ is the dimensionless similarity criterion of the given problem.

As a rule, in pumps $\Lambda < 0.3$. Therefore in Equation (A-11) the term $\Lambda^2 K$ is at least by an order of magnitude smaller than S .

Thus, for low harmonics of BPF pressure pulsations it is possible to drop the convective members in the wave equation:

$$\Lambda^2 \frac{\partial^2 \tilde{i}}{\partial \tilde{t}^2} - \tilde{\Delta} \tilde{i} = \tilde{S} \quad (\text{A-12})$$

For an undisturbed flow $\varphi = 0$ and:

$$\tilde{i}_0 = \tilde{j}_0 \quad (\text{A-13})$$

The functions i and j can be expressed through mean and pulsatory component:

$$\tilde{i} = \tilde{i}_0 + h; \tilde{j} = \tilde{j}_0 + g \quad (\text{A-14})$$

The amplitude of pressure pulsation in the pump is by an order of magnitude lower than the mean undisturbed pressure. Thus for enthalpy oscillations it is possible to write approximately:

$$h \approx \frac{(P - P_0)}{\rho_0 u_2^2} = \frac{P'}{\rho_0 u_2^2} \quad (\text{A-15})$$

Similarly for oscillations of the function g we obtain:

$$g \approx \frac{P'_v}{\rho_0 u_2^2} \quad (\text{A-16})$$

The last expression shows oscillations produced by nonstationary vortex motion of the medium (in the incompressible motion)—so-called “pseudosound.” Considering the formulae given by Equation (A-13), Equation (A-14), and Equation (A-15), we obtain from Equation (A-12) an equation of pressure oscillations (due to acoustical and vortex motion):

$$\Lambda^2 \frac{\partial^2 \tilde{i}}{\partial \tilde{t}^2} - \tilde{\Delta} \tilde{i} = \tilde{S} - \Lambda^2 \tilde{K} \quad (\text{A-17})$$

where $\tilde{S}' = -\Delta g$ is the nonstationary part of the function S .

Solution of Equation (A-17) is divided into two parts—computation of the incompressible flow for the determination of the disturbing function and solution of an inhomogeneous wave equation for the determination of h .

Discrete Vortex Method

The DVM concept is based on three main postulates:

- Turbulence is a vortices' motion (kinematics and transformation).

- In relation to our problem vortices mainly appear because of flow breaks from sharp edges and due to the wall layer separation (flow break).

- The transition from a deterministic flow to the turbulent one results in loss of stability of vortex structures (important for future simulations of turbulence pressure pulsation).

Physical Meaning of DVM

The fundamental formulation of DVM consists in the transformation of a continuous vortex sheet (tangential break) to distribution of discrete vortices.

The surface of tangential flow break (Figure A-1) is the limiting case for a vortex layer (sheet) with a vortex density $\gamma = V_{S2} - V_{S1}$. As $P_1 = P_2$ and $V_{n2} = V_{n1}$, centers of “elementary” vortices that form the vortex sheet, move at the velocity of flow, the circulation along a segment of sheet is constant. It is thus possible to replace the sheet with the set of discrete vortices of constant intensity:

$$\Gamma_k = \oint \gamma dl \quad (\text{A-18})$$

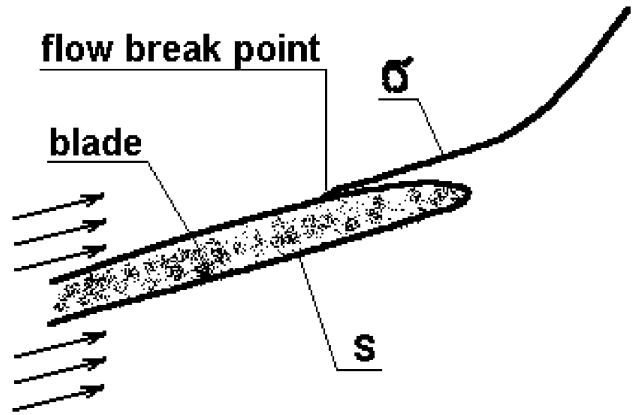


Figure A-1. Tangential Flow Break.

These are so-called free discrete vortices. They move with the flow.

The physical meaning of the vortex is very straightforward: following Stokes we can obtain:

$$\Gamma_k = \frac{l_{dv}}{l} \oint \vec{V} dl = \iint_A \text{rot} \vec{V} dA = 2 \iint_A \omega dA = \gamma l_{dv} \quad (\text{A-19})$$

The velocity at a point α can be found from relations:

$$\begin{aligned} U_{xa} &= \frac{1}{2\pi} \sum_k \Gamma_k \frac{y_a - y_r}{r_{ak}^2} \\ U_{ya} &= -\frac{1}{2\pi} \sum_k \Gamma_k \frac{x_a - x_r}{r_{ak}^2} \end{aligned} \quad (\text{A-20})$$

Intensity of the wall vortices is derived from the condition of impenetrability and condition of constant circulation (Thompson theorem). When finding Γ_j and Γ_k on S and σ it is possible to find the potential of flow and velocity field.

Criteria of Flow Separation

In the separated flow, it is necessary to define criteria of flow separation that follows the vortex generation (Figure A-2).

Under flow separation, we mean the process when the liquid detaches from the wall with a nonzero velocity. Therefore, the S and σ are tangent at the flow break point. At this point between σ and S , the velocity of liquid is equal to the velocity of motion of the break point.

The velocity of a free discrete vortex roll off is $\gamma^*/2$ where γ^* is the vorticity on σ at the break point.

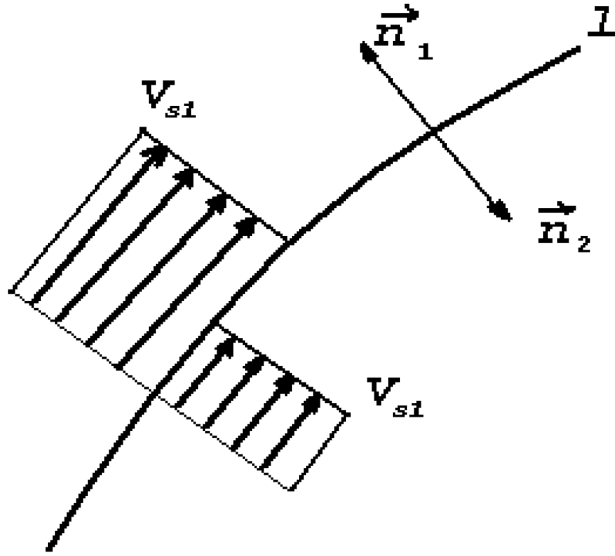


Figure A-2. Flow Separation with Creation of a Free Vortex Sheet σ .

Vorticity at the break point is defined by the formula:

$$\frac{d\gamma^*}{dt} = -\gamma^* \left(\frac{\partial V_{s1}^*}{\partial S} + \frac{\partial V_{n1}^*}{r^*} \right) \quad (\text{A-21})$$

where:

r^* = Curvature radius of σ
 V_{s1}^* and V_{n1}^* = Tangential and normal velocities of σ in the flow break point

Definition of the Problem

The statement of problem can be formulated as follows: in an unbounded incompressible unviscous liquid there is a finite number of velocity tangential breaks, which behave as blade surfaces $\Sigma(x, y, t)$ or as free sheets $\sigma(x, y, t)$ caused by the flow separation from blade surfaces. At the origin of the coordinates, there is the specific point—vortex-source $Q_0 - i\Gamma_0$. Except of the mentioned features, the flow has a potential, satisfying the Laplace equation:

$$\Delta\Phi = 0 \quad (\text{A-22})$$

Boundary conditions on the blade surfaces Σ are conditions of impenetrability. Boundary conditions on the free sheets σ are conditions of continuity of pressure and normal velocity (impenetrability condition) under transition from one hand of sheet to another one:

$$p_1 = p_2, (\nabla\Phi \cdot n)_1 = (\nabla\Phi \cdot n)_2. \quad (\text{A-23})$$

At infinity the liquid is at rest:

$$\lim \nabla\Phi = 0, x \rightarrow \pm\infty, y \rightarrow \pm\infty. \quad (\text{A-24})$$

It is possible to define Σ and σ as a finite number of discrete vortices Γ_j and Γ_k to determine Φ at an arbitrary point. The following formulas serve the determination of velocity field:

$$U_x = \frac{Q_0 y - \Gamma_0 x}{2\pi R^2} - \sum_{k,j} \frac{\Gamma_{k,j} z_i (\gamma_{k,j}^i)^{2i} \left\{ \frac{1}{2} (\gamma_{k,j}^i)^{2i} + \frac{1}{2} \sin[z_i(\theta - \theta_{k,j})] - \frac{1}{2} \cos[z_i(\theta - \theta_{k,j})] \right\}}{2\pi R \left\{ 1 - 2(\gamma_{k,j}^i)^{2i} \cos[z_i(\theta - \theta_{k,j})] + (\gamma_{k,j}^i)^{2i} \right\}} \quad (\text{A-25})$$

$$U_y = \frac{Q_0 x - \Gamma_0 y}{2\pi R^2} - \sum_{k,j} \frac{\Gamma_{k,j} z_i (\gamma_{k,j}^i)^{2i} \left\{ \frac{1}{2} (\gamma_{k,j}^i)^{2i} - \frac{1}{2} \cos[z_i(\theta - \theta_{k,j})] - \frac{1}{2} \sin[z_i(\theta - \theta_{k,j})] \right\}}{2\pi R \left\{ 1 - 2(\gamma_{k,j}^i)^{2i} \cos[z_i(\theta - \theta_{k,j})] + (\gamma_{k,j}^i)^{2i} \right\}} \quad (\text{A-26})$$

where:

x, y, θ, R = Coordinates of point, where velocity is defined

$\Gamma_{k,j}, \theta_{k,j}$ = Polar coordinates of discrete vortex $\Gamma_{k,j}$

Finite Difference Methods

For the numerical solution of the acoustic-vortex equations, nonstationary finite-difference methods are used. Mathematical domain representing the pump region is covered by a uniform rectangular grid (i, j) with steps $\Delta\eta, \Delta\xi$. Time points (k, l) with a step $\Delta\tau_v$ for vortex mode equations and with a step $\Delta\tau_a$ for wave equation are used. Introduction of different time resolution in two equations provides substantial economy in machine time and computer memory, from the stability conditions $\Delta\tau_a < \Delta\tau_v$ approximately by two orders. The ζ -equation is solved with a modified "second upwind scheme," and for Ψ -equation an elastic-viscous-plastic method ("EVP method") or a fast semi-implicit algorithm is applied. Pressure fluctuation is computed by means of a direct method. Finite-difference analogue of differential equations in the inner grid nodes is expressed by the formulae:

$$h_{i,j}^{l+1} = 2h_{i,j}^l - h_{i,j}^{l-1} + \frac{\Delta\tau_a^2}{\Lambda^2 E_j^2} \left(\frac{h_{i,j+1}^l - 2h_{i,j}^l + h_{i,j-1}^l}{\Delta\xi^2} + \frac{h_{i+1,j}^l - 2h_{i,j}^l + h_{i-1,j}^l}{\Delta\eta^2} \right) + \frac{\Delta\tau_a^2}{\Lambda^2} S_{i,j}^l \quad (\text{A-27})$$

$$\Psi_{i,j+1}^k = -(\Delta\xi E_j)^2 \zeta_{i,j}^k + 2 \left(1 + \frac{\Delta\xi^2}{\Delta\eta^2} \right) \Psi_{i,j}^k - \frac{\Delta\xi^2}{\Delta\eta^2} (\Psi_{i+1,j}^k - \Psi_{i-1,j}^k) - \Psi_{i,j}^k \quad (\text{A-28})$$

$$\zeta_{i,j}^{k+1} = \zeta_{i,j}^k - \frac{\pi \cdot \Delta\tau_v}{2z_i E_j^2 \Delta\eta \cdot \Delta\xi} \{ C_1 \times \zeta_1 - C_2 \times \zeta_2 + C_3 \times \zeta_3 - C_4 \times \zeta_4 \} \quad (\text{A-29})$$

$$\begin{aligned} C_1 &= \Psi_{i+1,j-1}^k - \Psi_{i+1,j+1}^k + \Psi_{i,j-1}^k - \Psi_{i,j-1}^k \\ C_2 &= \Psi_{i,j-1}^k - \Psi_{i,j+1}^k + \Psi_{i-1,j-1}^k - \Psi_{i-1,j-1}^k \\ C_3 &= \Psi_{i+1,j+1}^k - \Psi_{i-1,j+1}^k + \Psi_{i+1,j}^k - \Psi_{i-1,j}^k \\ C_4 &= \Psi_{i+1,j}^k - \Psi_{i-1,j}^k + \Psi_{i+1,j-1}^k - \Psi_{i-1,j-1}^k \end{aligned} \quad (\text{A-30})$$

if $(C_1 > 0) \zeta_1 = \zeta_{i,j}^k$ else $\zeta_1 = \zeta_{i+1,j}^k$

if $(C_2 > 0) \zeta_2 = \zeta_{i-1,j}^k$ else $\zeta_2 = \zeta_{i,j}^k$

if $(C_3 > 0) \zeta_3 = \zeta_{i,j}^k$ else $\zeta_3 = \zeta_{i,j+1}^k$

if $(C_4 > 0) \zeta_4 = \zeta_{i,j-1}^k$ else $\zeta_4 = \zeta_{i,j}^k$

Stability Conditions

The following inequalities define the limits of the time step for vortex mode equation ($\Delta\tau_v$) and for wave equation ($\Delta\tau_a$):

$$\frac{2\pi}{\gamma \cdot z_1} \left(\frac{|u_\eta|}{\Delta\eta} + \frac{|u_\xi|}{\Delta\xi} \right) \Delta\tau_v \leq 1 \quad (\text{A-31})$$

$$\frac{1}{\gamma^2 \Lambda^2} \left(\frac{1}{\Delta\eta^2} + \frac{1}{\Delta\xi^2} \right) \Delta\tau_a^2 \leq 1$$

Convergence Criteria

Convergence of the iteration process for the vortex mode is controlled with two criteria:

$$\begin{aligned} X_1^k &= \sum_{i,j} \left(\left| \frac{\zeta_{i,j}^k}{\zeta_{i,j}^{k-N}} \right| - \left| \zeta_{i,j}^{k-N} \right| \right) \\ X_2^k &= \max_{i,j} \left(\left| \Psi_{i,j}^k - \Psi_{i,j}^{k-N} \right| \right) \end{aligned} \quad (\text{A-32})$$

where:

k = Current time point

$k-N$ = Time point shifted back by one oscillation period

N = Number of time points in the oscillation period

The convergence condition under the first criterion $X_1^k \leq \epsilon_1$ is checked after each impeller turn. If the condition is reached, then

X_2^k is calculated for the second check— $X_2^k \leq \varepsilon_2$ (ε_1 , ε_2 are constants). The convergence condition for the wave solution is $X_3^k \leq \varepsilon_3$ (ε_3 is a constant) where:

$$X_3^k = \max_{i,j} \left(\left| h_{i,j}^l - h_{i,j}^{l-M} \right| \right) / \max_{i,j} \left(\left| h_{i,j}^0 \right| \right) \quad (\text{A-33})$$

where:

l = Current time point

$l-M$ = Time point shifted back by one oscillation period

M = Number of time points in the oscillation period

REFERENCES

- Chen, Y. N., 1961, "Water-Pressure Oscillations in the Volute Casings of Storage Pumps," Sulzer Technical Review, Research Number.
- Chu, S., Dong, R., and Katz, J., 1993, "The Effect of Blade-Tongue Interactions on the Flow Structure, Pressure Fluctuations and Noise Within a Centrifugal Pump," Pump Noise and Vibration, First International Symposium, Clamart, France, pp. 13-34.
- Croba, D. and Kueny, J. L., 1992, "Unsteady Flow Computation in a Centrifugal Pump Coupling of the Impeller and the Volute," Fan Noise, An International INCE Symposium, Senlis, France, pp. 221-228.
- Croba, D., Kueny, J. L., Hureau, F., and Kermarec, J., "Numerical and Experimental Unsteady Flow Analysis in Centrifugal Pumps," Impeller and Volute Interaction, Pump Noise and Vibration, First International Symposium, Clamart, France, pp. 111-119.
- Joffe, T. L. and Panchenko V. I., 1972, "To the Study of Influence of the Number of Impeller Blades of a Hydrodynamic Machine on Its Vibration-Acoustic Characteristics," Mashinovedeniye, (1).
- Sukup, J. K., 1974, "To the Problem of Pressure Pulsations in the Radial Centrifugal Pump," Translation No. 30915, Moscow, Russia (All-Union Center of Translations).
- Sukup, J. K., 1975, "To the Problem of Pressure Pulsations in the Centrifugal Pump," Translation No. 62734, Moscow, Russia (All-Union Center of Translations).
- Thompson, M. C., Hourigan, K., and Stokes, A. N., 1992, "Prediction of the Noise Generation in a Centrifugal Fan by Solution of the Acoustic Wave Equation," Fan Noise, An International INCE Symposium, Senlis, France, pp. 197-204.
- Touret, J., Kamga, M., Godefroi, B., Pluioise, M., Kermarec, J., and Bertinier, M., 1991, "Hydraulic Noise Generation Studies in Centrifugal Turbomachine Through Visualization of the Non Stationary Pressure Field in the Volute and in the Impeller," ASME/Reprinted from FED 128, *Experimental and Numerical Flow Visualization*, Editors: B. Khalighi, etc./Book No. 1991, pp. 239-246.
- Zogg, H. and Bolleter, U., 1993, "Generation and Propagation of Hydraulic Noise in Centrifugal Pumps," Pump Noise and Vibration, First International Symposium, Clamart, France, Proceedings, pp. 263-270.

Additional information for the specialized software package used in this paper can be retrieved from the website: www.pump-harmony.ru

BIBLIOGRAPHY

- Blokhintsev, D. I., 1981, "Acoustics of the Heterogeneous Moving Medium, Science, Moscow, Russia.
- Crow, S. C., 1970, "Aerodynamic Sound Emission as a Singular Perturbation Problem," *Studies in Applied Mathematics*, XLIX, (1).
- ISO 3740, 2000, "Acoustics—Determination of Sound Power Levels of Noise Sources—Guidelines for the Use of Basic Standards," International Organization for Standardization, Geneva, Switzerland.
- Landau, L. D. and Lifschitz, Y. E. M., 1954, *Continuum Mechanics*, Moscow, Russia: State Publishing House of Technical and Theoretical Literature.
- Ovsyannikov, B. V. and Timouchev, S. F., 1986, "About the Calculation of Pressure Pulsations on Blade Passing Frequencies in the Outlet of Centrifugal Pumps," In the Collection: "Problems of the Theory of Engines During Engine Testing," Moscow Aviation Institute (Chair 202).
- Timouchev, S. F., 1999, "Numerical Method and Software Package for Prediction of Pressure Pulsation in Centrifugal Ventilators," Forum Acusticum '99, The First Joint Meeting of EAA and ASA, Berlin, Germany, In a collection of abstracts.
- Timouchev, S. F. and Illichov, K. P., 1995, "2D Numerical Simulation of Unsteady Pressure Field in Centrifugal Pumps," Euro-Noise '95, An International INSE Symposium, Lyon, France, Proceedings, 3, pp. 905-910.
- Timushev, S. F. and Nedashkovsky, A. K., 1995, "Computational and Experimental Study of Acoustical Resonances in Centrifugal Pump Working Cavity," Pump Noise and Vibration, First International Symposium, Clamart, France, pp. 271-277.
- Timushev, S. F. and Ovsyannikov, B.V., 1992, "Pressure Fluctuation Numerical Simulation in a Centrifugal Pump Volute Casing," Journal de Physique IV, 2, Second French Conference on Acoustics, Arcachon, France, pp. 619-622.
- Timouchev, S. F. and Tourret, J., 1999, "Numerical Prediction of BPF Pressure Pulsation in Centrifugal Pumps and Ventilators with Harmony MK1, MK2 Software Packages," Ninth IAHR WG International Meeting on the Behavior of Hydraulic Machinery under Steady Oscillatory Conditions, Brno, Czech Republic, In a collection of papers.
- Timouchev, S. F. and Tourret, J., 2000, "Harmony Software for Low Noise Design of Centrifugal Ventilators of Transport Machines," Twenty-Ninth International Congress on Noise Control Engineering—InterNoise 2000, Nice, France, Proceedings, 6, pp. 3833-3836.
- Timouchev, S. F., Nedashkovsky, A., and Pavic, G., 1997, "Computational Study of the Acoustic Impedance Effect on BPF Pressure Oscillations in Centrifugal Pumps," Eighth IAHR WG International Meeting on the Behavior of Hydraulic Machinery under Steady Oscillatory Conditions, Chatou, France, In a collection of papers.

